HHS Public Access

Author manuscript

Cell Stem Cell. Author manuscript; available in PMC 2024 July 06.

Published in final edited form as:

Cell Stem Cell. 2023 July 06; 30(7): 950–961.e7. doi:10.1016/j.stem.2023.06.006.

Generating high-fidelity cochlear organoids from human pluripotent stem cells

Stephen T. Moore[1], **Takashi Nakamura**[1,2], **Jing Nie**[1], **Alexander J. Solivais**[1], **Isabel Aristizábal-Ramírez**[3], **Yoshitomo Ueda**[1], **Mayakannan Manikandan**[1], **V. Shweta Reddy**[1,4], **Daniel R. Romano**[1], **John R. Hoffman**[1], **Benjamin J. Perrin**[5], **Rick F. Nelson**[1], **Gregory I. Frolenkov**[3], **Susana M. Chuva de Sousa Lopes**[6], **Eri Hashino**[1,4,7,*]

[1]Department of Otolaryngology-Head and Neck Surgery, Indiana University School of Medicine, Indianapolis, Indiana 46202, USA.

[2]Department of Otolaryngology-Head & Neck Surgery, Kyoto Prefectural University of Medicine, Kyoto, Japan.

[3]Department of Physiology, University of Kentucky, Lexington, Kentucky 40536, USA.

[4]Stark Neurosciences Research Institute, Indiana University School of Medicine, Indianapolis, Indiana 46202, USA.

[5]Department of Biology, Purdue School of Science, Indianapolis, Indiana 46202, USA

[6]Department of Anatomy and Embryology, Leiden University Medical Center, Leiden, the Netherlands

[7]Department of Anatomy and Cell Biology, Indiana University School of Medicine, Indianapolis, Indiana 46202, USA.

SUMMARY

Mechanosensitive hair cells in the cochlea are responsible for hearing, but are vulnerable to damage by genetic mutations and environmental insults. The paucity of human cochlear tissues makes it difficult to study cochlear hair cells. Organoids offer a compelling platform to study scarce tissues in vitro; however, derivation of cochlear cell types has proven non-trivial. Here, using 3D cultures of human pluripotent stem cells, we sought to replicate key differentiation cues of cochlear specification. We found that timed modulations of Sonic Hedgehog and WNT

*Further information and requests for resources and reagents should be directed to and will be fulfilled by the lead contact, Eri Hashino (ehashino@iu.edu).

AUTHOR CONTRIBUTIONS

Conceptualization, E.H. and S.T.M.; Methodology, S.T.M., T.N., J.N.; Investigation, S.T.M., T.N., J.N., I.A.R., Y.U., M.M., V.S.R., S.M.C.S.L.; Data Curation, A.J.S., D.R.R. and J.R.H.; Writing – Original Draft, E.H., S.T.M., J.N., A.J.S. and G.I.F.; Writing – Review & Editing, T.N., R.F.N. and S.M.C.S.L.; Funding Acquisition, E.H.; Resources, B.J.P., R.F.N. and S.M.C.S.L.; Supervision, E.H., G.I.F. and S.M.C.S.L.

DECLARATION OF INTERESTS

S.T.M. and E.H. are the inventors on a PCT patent application titled "*Methods of generating human cochlear hair cells*". The other authors declare no competing interests.

signalling promote ventral gene expression in otic progenitors. Ventralized otic progenitors subsequently give rise to elaborately patterned epithelia containing hair cells with morphology, marker expression, and functional properties consistent with both outer and inner hair cells in the cochlea. These results suggest that early morphogenic cues are sufficient to drive cochlear induction and establish an unprecedented system to model the human auditory organ.

eTOC Blurb

Moore and colleagues present a protocol for generating cochlear organoids from human PSCs by treating otic progenitors with ventralization signals. Derived hair cells in cochlear organoids exhibit molecular, structural and functional features of cochlear hair cells, and serve as a model to study how sound-sensing hair cells in humans develop.

Graphical Abstract

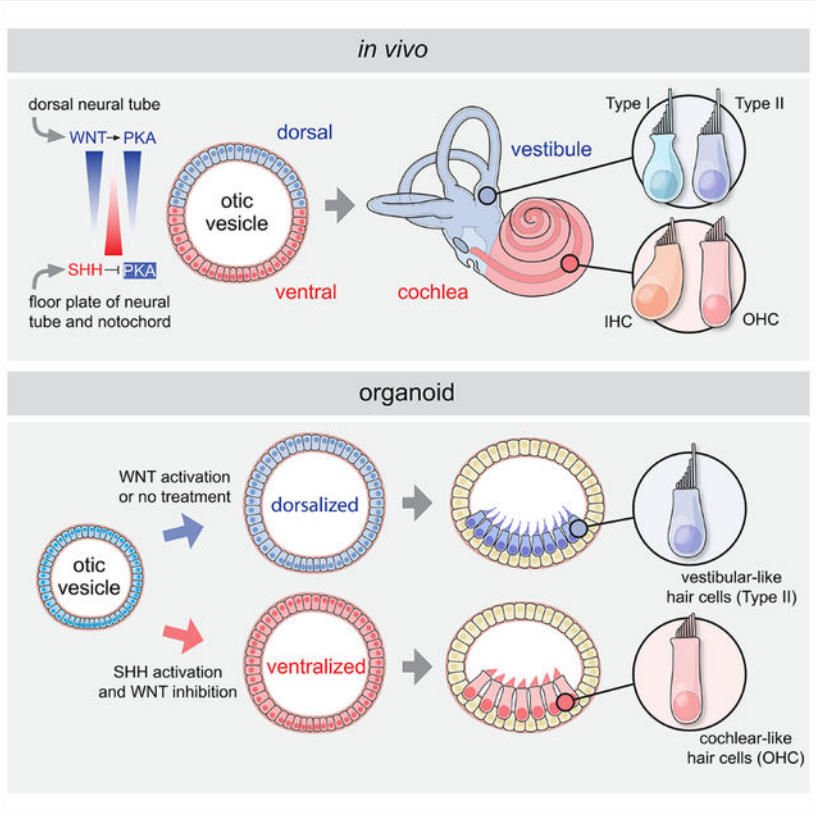

INTRODUCTION

The human inner ear is among the most elaborate organs in nature; featuring the spiral-shaped cochlea with its orderly rows of sound-detecting sensory cells and the intricate labyrinth of the vestibular organs that confer the sense of balance. The astonishing complexity of inner ear morphogenesis is orchestrated by a symphony of interwoven signalling events during fetal development that proceeds with remarkable fidelity [1–3]. Indeed, while almost 10% of adults have moderate-to-profound hearing loss, the incidence at

birth is less than 0.2%, meaning that the vast majority of sensorineural hearing loss results from the post-natal death or dysfunction of cells within a developmentally pristine inner ear [4].

To recapitulate the intricate process of human inner ear development *in vitro*, we and others previously established defined 3D culture systems to generate inner ear sensory epithelia from aggregates of mouse or human pluripotent stem cells [5–10]. These so-called "inner ear organoids" harbour a layer of supporting cells and functional hair cells that are innervated by sensory-like neurons. Although these organoids consistently generate hair cells with structural, biochemical and functional properties comparable to native vestibular hair cells, they lack any cochlear cell types. To address the need for better tools to study human inner ear development and disease, we sought to establish a new organoid system that gives rise to cochlear cell types, including inner and outer hair cells, which are the functional unit of auditory mechanosensation.

RESULTS

A multiplex reporter hESC line provides enhanced culture optimization

To monitor the derivation of otic progenitors and hair cells in culture and improve the efficiency of our previously published protocols [5,8] we generated a *PAX2*-2A-nGFP/*POU4F3*-2A-ntdTomato reporter human embryonic stem cell (hESC) line using the CRISPR/Cas9 genome engineering technology. PAX2 is an early marker of otic progenitors *in vivo,* while POU4F3 expression is highly specific to hair cells and provides a late-stage readout of culture efficiency [11–13]. We first confirmed that PAX2b is the most abundantly expressed PAX2 isoform in human inner ear organoid tissues (Figures S1A–B). Using a high-fidelity Cas9 [14] and a sgRNA targeting the stop codon of this isoform, we knocked in a 2A-nGFP cassette immediately downstream of the endogenous *PAX2* coding sequence (Figures 1A, S1C–D; Table S1). A 2A-ntdTomato cassette was similarly knocked in to the *POU4F3* locus downstream of the *POU4F3* stop codon using the established *PAX2*-2A-nGFP hESCs as a parental cell line (Figures 1A, S1G–H; Table S1). The resulting multiplex reporter cell line expressing multiple pluripotency markers (Figure S1E) labels the *PAX2*+ otic progenitors with nuclear GFP starting from around organoid culture day 12 (D12), and the *POU4F3*+ hair cells with nuclear tdTomato starting from around D35 (Figures 1B–L, S1F, I–L"; Video S1). Using the hESC reporter line we had established, we systematically changed basal media, timings and durations of small molecule treatment to optimize otic induction (Figure 2A). Following optimization, the number of *POU4F3*-positive aggregates more than doubled vs. our previous protocols [8,15], and the average *POU4F3*-positive area per aggregate increased ~20-fold (Figures 2B and 2C).

Sequential modulations of Sonic Hedgehog and WNT signaling promote ventralization of inner ear organoids

During inner ear development, the cochlear structure is derived from the most ventral region of the otic vesicle, whereas the vestibular structures originate from a more dorsal otic region [1] (Figure 3A). Our culture platform relies in part on self-guided differentiation and patterning, and similar to previously reported inner ear organoid protocols [8,9,15,16],

our optimized basal control (CTRL) culture system consistently generates hair cells with a vestibular phenotype. We hypothesized that, as in embryonic development, signals exogenous to the otocyst may be necessary for cochlear induction. Sonic Hedgehog (SHH), a signaling molecule secreted from the floor plate of the neural tube and underlying notochord, is essential for patterning of the ventral otic vesicle. SHH is necessary to ventralize the otocyst and derive cochlear structures in mice and chicks [17,18]. In contrast, the WNT signaling pathway has been shown to play a role in induction of dorsal gene expression during inner ear development [19,20].

Based on these previous mouse genetics studies, we hypothesized that timed activation of the SHH pathway, with concomitant suppression of WNT signaling may promote upregulation of ventral otic genes, leading to generation of cochlear hair cells in long-term culture (Figure 3A). To examine this hypothesis, we cultured hESC-derived organoids containing otic progenitors in the presence of the small molecule SHH agonist purmorphamine (PUR) alone, in combinations with the WNT inhibitor IWP2 (PUR+IWP2), or neither (CTRL) (Figure 3A). All conditions followed our optimized differentiation protocol to obtain otic progenitors, and differed only in the presence or absence of the noted small molecules.

We performed single-cell RNA-sequencing (scRNA-seq) analysis on D20 *PAX2*-nGFP+ sorted cells from aggregates generated under CTRL, PUR or PUR+IWP2 conditions (Figure S2A–E). Each condition was analysed separately, one batch per condition. A total of 37,073 cells were collected, and the cells from each batch were merged and clustered together. Unbiased clustering, as implemented in Seurat v3.2, revealed that *EPCAM*+/*FBXO2*+ otic progenitors from the PUR+IWP2 condition formed a distinct cluster, whereas PUR and CTRL otic progenitors clustered together (Figure 3B). Otic progenitors from all three conditions were isolated, and subsequent differential expression analysis among conditions revealed that dorsal otic markers such as *DLX5*, *MSX1*, *GPR166*, and *ACSL4*, were largely confined to PUR and CTRL treated cells, whereas ventral otic markers, including *OTX1/2*, *NR2F1/2*, *EDN3*, and *RSPO3* were concentrated in the PUR+IWP2 condition. Moreover, genes involved in the SHH-pathway, such as *SULF1*, *LRP2*, *GAS1*, and *PTCH1* were highly expressed in the PUR+IWP2-treated cells, but their expression was attenuated in CTRL and PUR-treated progenitors (Figure 3C). Consistent with this, Gene Set Enrichment Analysis (GSEA) [21] revealed enrichment of gene sets associated with the Hedgehog pathway and downregulation of gene sets associated with the canonical WNT pathway in PUR+IWP2 treated otic progenitors when compared to untreated CTRL otic progenitors. Additionally, analysis of PUR+IWP2 treated otic progenitors revealed multiple enriched gene sets for posttranscriptional regulation of gene expression, chromatin modifications, and gene sets composed of the targets of known hereditary deafness genes coding for transcription factors such as *ZNF711*, *MORC2*, *GCM2* and *BARHL1* (Figure 3D). These finding are suggestive of a developmental trajectory that is divergent from CTRL and PUR conditions, with enrichment for genetic programs linked to establishment and maintenance of hearing. We substantiated the scRNA-seq data with immunofluorescence for NR2F1, SULF1, OTX2 and DLX5 using D25 organoids (Figures 3E and S2F–G). We concluded that a more efficient ventralization of hESC-derived otic progenitors after sequential treatment with PUR and IWP2 is due to, at least partially, modulation of SHH down-stream gene targets. Since

protein kinase A (PKA) has been shown to act as a negative SHH mediator [18], we examined effects of the small molecule H89, a cell-permeable PKA inhibitor, alone or in combination with PUR and IWP2, but none of these treatments were efficacious in deriving hair cells (Figure S3).

Otic progenitors in ventralized inner ear organoids give rise to cochlear hair cells

PUR+IWP2-treated and CTRL aggregates were grown in defined culture medium devoid of exogenous signalling molecules or growth factors from D22 onward. To compare the transcriptional profile between PUR+IWP2-treated and CTRL hair cells, D80 and −109 *POU4F3*+ sorted cells were analysed via scRNA-seq (Figures 4, S4). We employed a non-stringent FACS gating strategy to collect high and low *POU4F3*-expressing cells, which resulted in recovering sequence data from 3,332 hair cells (18.9% of total 17,668 cells) and 4,582 hair cells (28.6% of total 16,044 cells) for D80 and −109 samples, respectively. Similar to D20 scRNA-seq data, PUR+IWP2 hair cells separated out from CTRL hair cells when the cells were subjected to unbiased clustering (Figures 4B–E, S4A, C, E). The volcano plot showing differentially expressed genes between the two conditions identified several known cochlear hair cell markers [22–25], including *GATA3*, *INSM1*, *HES6*, *TMPRSS3* and *GNG8*, whose expression was significantly higher in PUR+IWP2-treated vs. CTRL hair cells at D109 (Figures 5A–B). Consistent with our scRNA-seq data, immunofluorescence of PUR+IWP2-treated organoids showed that *POU4F3*+ cells express significantly higher levels of cochlear hair cell marker proteins, such as NR2F1 and GATA3 (Figures 5C–D; Video S2), which was confirmed in hair cells of fetal human cochleae at gestation week (GW) 18 (Figure 5E).

We used scanning electron microscopy to compare the structural properties of hair bundles on the apical surface of derived hair cells between PUR+IWP2 and CTRL organoids (Figures 6A–H’). Structural development of the hair bundle - from the emergence of a kinocilium in the middle of the cuticular plate to development of a stair-cased pattern of stereocilia [26], typically seen in the mouse inner ear, was observed in organoid hair cells (Figures S5A–C). We also detected tip-link-like structures between individual stereocilia (Figure S5C’–C”). These transitional properties recapitulate development of the hair bundle in mouse cochleae. In CTRL organoids at D110–200, we consistently observed long pointed arrangement of hair bundles, characteristic of vestibular hair cells. In striking contrast, the length of hair bundles was significantly shorter in PUR+IWP2-treated samples and stereocilia were often arranged in a linear or concave geometry, reminiscent of stereocilia on the apical surface of inner hair cells in the mouse cochlea (Figures 6A–H and S5H–I). High-resolution confocal microscopy substantiated these results by showing differences in the arrangement and overall length of stereocilia between PUR+IWP2-treated and untreated CTRL hair cells (Figures 6I–L and S5E–F, L–M). Native cochlear hair bundles feature narrow stereocilia in the front rows with larger diameters in the middle and back rows, while vestibular stereocilia are more uniform. PUR+IWP2-treated hair bundles also featured a gradient of stereocilia diameters, while CTRL stereocilia were uniform along their varying lengths s (Figures 6M, S5D–D’, J–K). These structural differences in the hair bundle between PUR+IWP2 and control hair cells are consistent with structural differences observed between cochlear and vestibular hair cells in the mammalian inner ear. TUJ1+

neurite processes infiltrating sensory epithelia and contacting the basolateral region of hair cells were observed in both PUR+IWP2 and control organoids (Figures S5G, N), suggesting development of neural innervation in these organoids.

We tested the reproducibility of our new protocol using a human induced pluripotent stem cell (iPSC) line (mND2–0). As previously described[8], this line required a higher BMP4 concentration (2 ng/mL vs 1 ng/mL for the WA25 hESC line) to consistently produce epithelial vesicles (Figure S6A) due probably to the variability in endogenous BMP concentrations inherent to different pluripotent stem cell lines. Treating iPSC-derived aggregates with PUR and IWP2 resulted in abolished DLX5 expression and increased NR2F1 expression in PAX2+/PAX8+ vesicular cells in organoids at D25 (Figure S6B). At D82, all PCP4+ cells (presumably hair cells) and the surrounding cells (presumably supporting cells) expressed GATA3 in PUR+IWP2 samples, which was in striking contrast with a total lack of GATA3+ cells in PCP4+ vesicles of CTRL samples (Figure S6C). Similarly, NR2F1 was detected in all PCP4+ and surrounding cells in PUR+IWP2 organoids, but was undetectable in those in CTRL organoids. Confocal microscopy of D113 PUR+IWP2 hair cells uniformly exhibited short hair bundles (Figure S6D), consistent with our results obtained from hESC-derived organoids.

To assess the identity of PUR+IWP2-treated hair cells, we examined expression of PRESTIN, a hallmark of cochlear outer hair cells [27,28]. Membrane-localized PRESTIN was detectible in some samples as early as D102 (0.33% of hair cells), and expression becomes more widespread as cultures age. On D150 and 200, 12.6% and 16.8% of all PUR+IWP2-treated hair cells, respectively, express membrane-localized PRESTIN (Figures 7A–B). In contrast, PRESTIN was undetectable in any CTRL hair cells, up to D200 (Figure 7A). To assess functional development of PUR+IWP2-derived hair cells, we performed conventional whole cell patch clamp recordings of the voltage-activated ion conductances in the cells exhibiting strong tdTomato reporter signal (Figure 7C). Two functionally distinct types of cells were identified with K^+-based intracellular solution. The cells of the first group (type A) were observed more often (78%) and were characterized by fast outward currents and virtually no inward currents, similar to the mature outer cochlear hair cells [29]. Less frequent (22%) cells (type B) exhibited slow outward currents and prominent fast inward currents, reminiscent of K^+ and Na^+ currents in immature inner hair cells [29]. Both types of cells had similar reversal potential (mean = −34.7 mV, range from −17.5 to −55.5 mV) and showed no evidence of KCNQ-type fast K^+ current activated at resting potential [30].

To determine the identity of other cell populations arising in cochlear organoids, we performed scRNA-seq analysis of EPCAM+ and EPCAM− cell populations isolated from D81 PUR+IWP2 organoids. This approach increased the percentage of EPCAM+ cells, including hair cells and supporting cells, of all sampled cells for sequencing, which allowed for high-resolution analysis and clustering of otic epithelial cells. The merged dataset identified several clusters, including hair cell, supporting cell, otic epithelium, neuron and Schwann cell clusters (Figure S7A–D). The majority of cells in the hair cell, supporting cell and otic epithelial cell clusters were EPCAM-positive, while the other clusters contained both EPCAM-positive and -negative cells. Subclustering of the supporting cell cluster identified 2 cell populations with one representing *BRICD5*+/*SPARCL1*+ supporting cells

and another cell population expressing the stria vascularis markers *CLDN11*, *LRP2*, *DACH1* and *PTGDS* [31,32] (Figure S7E). Immunofluorescence for CLDN11 revealed its expression in epithelial regions of vesicles containing *POU4F3*+ hair cells (Figure S7F). The endolymphatic duct marker LMX1A [33,34] was absent in PUR+IWP2 organoids, but present in *POU4F3*− ductal structures of CTRL organoids (Figure S7G–G').

DISCUSSION

Existing protocols for inner ear organoids yield exclusively hair cells with structural, molecular, and physiological properties resembling those of vestibular hair cells. Thus, the goal of the present study was to develop a means to derive cochlear hair cell types in organoids. Since a gradient SHH concentration across the dorso-ventral axis of otic vesicles is considered a primary ventralizing cue during inner ear development, we first examined the effects of the potent smoothened agonist PUR on changes in gene expression in D20 organoids, however augmentation of the SHH pathway alone was not sufficient to promote ventral otic differentiation. In parallel, we co-treated hESC-derived aggregates with the WNT inhibitor IWP2 beginning five days into treatment with PUR. This treatment resulted in a significant upregulation of ventral otic markers, while suppressing dorsal otic markers. We also observed significant upregulation of SHH down-stream effectors, such as *SULF1*, *LRP2*, *GAS1* and *PTCH1*, in PUR+IWP2-treated samples, but not in CTRL or PUR-treated samples, suggesting that ventralization of otic progenitors requires a threshold of SHH pathway activation that includes upregulation of ligand receptors and down-stream effectors that are antagonized by WNT signaling.

Our scRNA-seq analyses of D80 and −109 samples revealed that PUR+IWP2 treated and untreated control hair cells exhibit distinctive transcriptional profiles. Of the differentially expressed genes between these two cell populations, *NR2F1* and *GATA3* were among the most highly expressed in PUR+IWP2 treated hair cells at both D80 and −109, suggesting these two genes as potential candidates for core elements in the transcriptional pathway leading to cochlear differentiation. GATA3 has been shown to be predominantly expressed in cochlear vs. vestibular tissues [35–37], but less is known about the role for the orphan nuclear receptors NR2F1/2 in cochlear specification. Targeted inactivation of *NR2F1* results in supernumerary hair cells and supporting cells in the developing mouse cochlea, which is associated with dysregulation of Notch signaling components [38]. NR2F1/2 are thought to function as ligand-dependent transcription factors, and as such might act as master drivers to confer multipotent otic progenitors with competence to differentiate into cochlear cell types. It is worth noting, however, that NR2F1/2 have been shown to play an essential role in dorso-ventral patterning of the optic vesicle through direct regulation of *OTX2* expression [39]. We consistently observed that the first sign of *POU4F3*+ cells in PUR+IWP2 treated organoids approximately 10 days later than that in control organoids. The delayed emergence of cochlear hair cells compared to the timing of vestibular hair cell emergence in organoids is consistent with the temporal order of hair cell differentiation in the mouse inner ear [40,41]. This suggests that vestibular and cochlear tissue differentiation is temporally controlled by yet-to-be defined mechanisms and that GATA3 and/or NR2F1/2 could be involved in temporal control of cochlear differentiation.

Our present results showing the differential expression of the stria vascularis marker CLDN11 in PUR+IWP2 organoids and the endolymphatic duct marker LMX1A in CTRL organoids suggest that nonsensory cell types in the cochlear or vestibular epithelia can be selectively derived by our PUR+IWP2 or CTRL organoid protocol. The stria vascularis, a vascularized tissue located in the lateral wall of the cochlea, acts to maintain cochlear homeostasis through CLDN11-dependent basal cell tight junctions and is essential for hearing [31,42,43]. Thus, establishing human cochlear epithelia containing not only hair cells and supporting cells, but also stria vascularis cells, would have a major impact on hearing research in the future, as they could serve as a more faithful model system to recapitulate development of sensory transduction in the cochlea. However, conformation of the presence of the stria vascularis in *POU4F3*+ vesicles of PUR+IWP2 organoids awaits further investigation on cellular composition and functional assessment. The presence of LMX1A in ductal structures of CTRL organoids and its absence in PUR+IWP2 organoids is consistent with the notion that the endolymphatic duct arises from the dorsal part of the otic vesicle during development [44,45].

We sought to further classify derived hair cells in ventralized inner ear organoids as either outer or inner cochlear hair cells. Structurally, these hair cells exhibit U-shaped hair bundles with short stereocilia bearing varying diameters, as typically seen in inner hair cells of the mammalian cochlea [46,47]. However, INSM1, a Zinc finger transcription factor essential for outer hair cell differentiation in the mouse [48], is predominantly expressed in hair cells of PUR+IWP2 treated organoids, while expression of *TBX2*, a pioneering factor for inner hair cell differentiation [49] is not significantly different between PUR+IWP2 and control hair cells. Additionally, our electrophysiological recordings identified two distinctive hair cell populations in D138–164 PUR+IWP2 organoids. Approximately 78% of these hair cells were characterized by fast outward currents and virtually no inward currents, which is similar to native outer but not inner hair cells in the mouse cochlea. Although this proportion is much higher than the 1.6% of hair cells that we detect expressing the outer hair cell marker *SLC26A5* (PRESTIN) in our scRNA-seq dataset at D109, immunofluorescence data suggests that the number of PRESTIN+ hair cells increase dramatically over time in PUR+IWP2 organoids from D102 to 200 (from 0.33% to 16.8%), which may explain the higher percentage of outer hair cell-like cells in our patch clamp recordings at D138-D164. This also indicates that derived hair cells may not have reached phenotypic maturation when the scRNA-seq experiments were performed. While we found multiple hallmarks of the outer hair cell identity, our data pointing to the inner hair cell identity are limited. Investigation is underway to determine if *bona fide* inner hair cells arise concomitantly with outer hair cells in these organoids.

Based on our transcriptional and structural analysis, the time course of hESC-derived cochlear organoid development closely parallels that of human cochlear development, with D110 inner ear organoids corresponding approximately to human fetal inner ears at GW18. Moreover, the order of marker expression is also faithfully recapitulated in inner ear organoids with *ATOH1* expression preceding *MYO7A* expression. PRESTIN is detected in outer hair cells of the human fetal cochlea at GW18, but absent at GW 13. Likewise, PRESTIN is detected in approximately 16% of hair cells in PUR+IWP2 treated organoids at D200, but is barely detectable at D102. These results suggest that the cochlear organoids

we have established in the present study can reach a developmental stage comparable to the human cochlea well into the third trimester.

In conclusion, we have demonstrated that precisely timed modulations of the SHH and WNT pathways confer multipotent otic progenitors with a ventral otic phenotype, some of which subsequently give rise to hair cells with structural, transcriptional and functional properties of the two types of cochlear hair cells, inner and outer hair cells and mature *in vitro* well into a stage corresponding the third trimester of human fetal development. Additionally, scRNA-seq analysis identifies NR2F1 as a previously unrecognized candidate for the key transcriptional pathway essential for cochlear and vestibular diversification. Further investigation is required to elucidate the mechanisms underlying the cross talk between the transcriptional pathways and structural development, and establish a means to control inner vs. outer hair cell generation. The cochlear organoids we have established in this study are expected to serve as a powerful human model to investigate the biology of human cochlear development, elucidate pathogenesis of hereditary hearing loss, and identify therapeutic targets to treat profound hearing loss.

Limitations of the Study

While the cochlear organoid system we have established in the present study is a valuable tool for studying human cochlear development, it lacks patterning pertinent to the snail-shaped cochlear organ. Moreover, the current system contains sensory epithelia and connecting neurons, but lacks entirely central nervous system components. Future studies overcoming these limitations are needed to develop a next-generation model system that recapitulates aspects of patterning and regional specificity as well as auditory neural circuitry.

STAR methods

RESOURCE AVAILABILITY

Lead Contact—Further information and requests for resources and reagents should be directed to and will be fulfilled by the lead contact, Eri Hashino (ehashino@iu.edu)

Material Availability—Research reagents generated in this study will be distributed upon request to other investigators under MTA.

Data and code availability—Single-cell RNA-seq data have been deposited at the Gene Expression Omnibus (GEO) and are publicly available as of the date of publication. Accession numbers are listed in the key resources table. Microscopy data reported in this paper will be shared by the lead contact upon request.

All original code has been deposited at the GitHub repository and is publicly available as of the date of publication. DOIs are listed in the key resources table.

Any additional information required to reanalyze the data reported in this paper is available from the lead contact upon request.

EXPERIMENTAL MODELS AND STUDY PARTICIPANT DETAILS

Human cell lines—We used the female human embryonic stem cell line WA25 (NIHhESC-12-0196, RRID:CVCL_E080) obtained from WiCell Research Institute as a parental cell line to generate the PAX2-2A-nGFP/POU4F3-2A-ntdTomato reporter stem cell line used throughout this study. We also used the male human induced pluripotent stem cell line mND2–0 (MIRJT7i-mND2-0,RRID:CVCL_U173) to repeat critical experiments. Cells were maintained and passaged in Essential 8 Flex Medium (Thermo Fisher, A2858501) supplemented with 100 μg/ml Normocin (E8fn) on recombinant human Vitronectin-N (Thermo Fisher, A14700)-coated 6-well plates at 37 C with 5% CO2. Media was replaced every other day and cells were passaged every 5–6 days using 0.5mM EDTA (Thermo Fisher). Cell lines were quality controlled with karyotyping, immunofluorescent labeling of pluripotency markers, and sequencing of predicted off-target regions after CRISPR/Cas9 gene editing.

Human tissues—Human fetal cochleae were collected and processed at the Leiden University Medical Center (Netherland) from tissues obtained from elective abortion using vacuum aspiration. Prior to the procedure, obstetric ultrasonography was performed to determine the gestational weeks (GW) and days. One GW 13 cochlear, one GW18 cochlear and one GW 18 vestibular samples were used in this study. The use of human fetal tissues was approved by the Medical Ethical Committee of the Leiden University Medical Center (Protocol Number 08.087). Informed written consents were obtained in accordance with the WMA Declaration of Helsinki guidelines.

METHOD DETAILS

Establishment of *PAX2/POU4F3* reporter hESC lines with CRISPR/Cas9—To monitor the derivation of otic progenitors in 3D culture, we generated *PAX2* reporter hESC lines by integrating a 2A-eGFP-nls (2A-nGFP) fluorescence reporter at the endogenous *PAX2* locus using the CRISPR/Cas9 genome engineering technology. Based on the locations of the stop codons, *PAX2* splicing variants can be grouped as Types PAX2b, PAX2c, and PAX2d [50–52]. Total RNA was isolated from D40 inner ear organoids by homogenizing whole aggregates in ice-cold TRIzol (Fisher, cat. no. 15596026) followed by chloroform extraction and isopropanol precipitation. A cDNA library was constructed using iScript cDNA synthesis kit following the manufacturer's suggested protocol (Biorad, Cat. No. 1708891). Standard PCR was performed on the cDNA library as well as on PAX2b, PAX2c, and PAX2d synthetic cDNA gBlocks (IDT) for size reference using primers 5'CCTGGCAGGAATGGTGCCT3' and 5'GTCAGACGGGGACGATGTGG3' targeting a common exon and the 3'UTR of PAX2. Agarose gel electrophoresis of the PCR amplicons followed by Sanger sequencing verification of the extracted brightest band showed that PAX2b was the most abundant type of *PAX2* isoforms in human inner ear organoids. Therefore, gRNA and homology arms were designed to target the PAX2b stop codon locus. To construct the *PAX2*-2A-eGFP-nls-pA-loxP-PGK-Puro-pA-loxP donor vector, two 1 kb homology arms flanking the PAX2b stop codon were PCR amplified from WA25 hESC (WiCell, derived from a female donor) genomic DNA. Gibson assembly [53] was used to connect the two homology arms with 2A-eGFP [8,54], nls-stop-bGH polyA (gBlock, IDT), and loxP-PGK-Puro-pA-loxP DNA fragments [8,54], as well as a linearized pUC19 plasmid

backbone into the final donor vector. gRNA (5'- ATGACCGCCACTAGTTACCG −3') targeting the PAX2b stop codon was cloned into an expression plasmid under the control of a U6 promoter (Addgene #71814) [55]. The *PAX2*-2A-nGFP donor vector, the PAX2b gRNA plasmid, as well as a high fidelity Cas9 expression plasmid (SpCas9-HF1, Addgene #72247) [14] were transfected into WA25 hESCs with 4D Nucleofector (Lonza) using the P3 Primary Cell 4D-Nucleofector X kit and Program CB-150. After nucleofection, cells were plated in E8fn medium containing 1× RevitaCell (Thermo Fisher) for improved cell survival rate, and 1 μM of Scr7 (Xcessbio) for higher HDR efficiency [56]. 0.5 μg/mL puromycin selection was performed for 14 days starting from 48 h post-nucleofection. The PGK-Puro sub-cassette flanked by two loxP sites was removed from the genome after puromycin selection by nucleofection of a Cre recombinase expressing vector (Addgene #13775)[57]. Clonal cell lines were established by low-density seeding (1–3 cells/cm^2) of dissociated single hESCs followed by isolation of hESC colonies after 5–7 d of expansion. Genotypes of the clonal cell lines were analysed by PCR amplification of genomic DNA isolated using the QuickExtract DNA Extraction Kit (Fischer Scientific, NC9904870), followed by gel electrophoresis, and by Sanger sequencing of total PCR amplicons or individual PCR amplicons cloned into TOPO vectors (Thermo Fisher). Cell lines with bi-allelic 2A-nGFP integration were used for subsequent experiments. Top 10 predicted off-target sites of the gRNA were PCR amplified (~1 kb) from the genomic DNA of the established cell lines and were Sanger sequenced to test for off-target mutations.

To build a *PAX2*-2A-nGFP/*POU4F3*-2A-ntdTomato multiplex reporter cell line, the *POU4F3*-2A-ntdTomato knockin CRISPR was performed on the *PAX2*-2A-nGFP genetic background. The *POU4F3*-2A-tdTomato-nls-bGH polyA-frt-PGK-Puro-pA-frt donor plasmid was constructed by connecting the following DNA fragments via Gibson assembly: Two 1 kb homology arms flanking the *POU4F3* stop codon amplified from WA25 genomic DNA, 2A-tdTomato gBlock DNA, nls-stop-bGH pA gBlock DNA, frt-PGK-Puro-frt gBlock DNA (IDT), and a linearized pUC19 backbone. The completed donor plasmid was transfected into the *PAX2*-2A-nGFP parental hES cell line along with a ribonucleoprotein complex composed of a synthetic sgRNA (5'- ATTCGGCTGTCCACTGATTG - 3') (Synthego) targeting the *POU4F3* stop codon locus, and a high fidelity Cas9 protein (HiFi Cas9 v3, IDT). The transfection was also performed with a 4D Nucleofector (Lonza) using the P3 Primary Cell 4D-Nucleofector X kit and Program CB-150. After nucleofection, cells were plated in E8fn medium containing 1× RevitaCell (Thermo Fisher) and 1 μM of Scr7 (Xcessbio). 0.5 μg/mL puromycin selection was performed for 9 days starting from 48 h post-nucleofection. The frt-flanked PGK-Puro cassette was removed via FLPo transfection (Addgene #13793)[58]. Clonal cell line isolation and genotyping procedures were the same as *PAX2*-2A-nGFP CRISPR. The final multiplex cell line chosen for downstream experiments had bi-allelic 2A-nGFP knockin at the *PAX2* locus and bi-allelic 2A-ntdTomato knockin at the *POU4F3* locus, and was karyotyped by the KaryoLogic Inc. (Research Triangle Park, North Carolina).

Organoid culture—*PAX2*-2A-nGFP/*POU4F3*-2A-ntdTomat hESCs (passages 22–50) or mND2–0 human iPSCs (WiCell, derived from a male donor, passages 33–50) were maintained and passaged in Essential 8 Flex Medium (Thermo Fisher, A2858501)

supplemented with 100 μg/ml Normocin (E8fn) on recombinant human Vitronectin-N (Thermo Fisher, A14700)-coated 6-well plates. Human inner ear organoids were derived from hESCs based on our previous protocol [8,15] with major modifications. Briefly, hESCs were dissociated with StemPro Accutase (Thermo Fisher, A1110501) and distributed at 3500 cells per well onto low-adhesion 96-well U-bottom plates in 100 μL E8fn containing 20 μM Y-27632 (Stemgent, 04–0012-02) and centrifuged at 120 g for 5 minutes. 100 μL of E8fn was added to each well following 4h of incubation. After 48h of incubation, induction of non-neural epithelium (differentiation day zero), proceeded as follows: aggregates were transferred to a 10 cm dish using a multichannel pipette, the plate was gently swirled to collect aggregates in the center, then samples were transferred to a 2 mL tube using a wide-orifice P1000 pipette. Aggregates were then washed 3 times in DMEM:F12 with HEPES buffer (Thermo Fisher, 11320033) to remove all E8fn, and a further 3 times with new differentiation media made from E6 medium (Thermo Fisher, A1516401) with Normocin (E6n) containing 4 ng mL^{-1} FGF-2 (StemCell Technologies, 780003), 10 μM SB-431542 (Stemgent, 04–0010-05), and 2% growth factor reduced (GFR) Matrigel (Corning, 354230), and 1–2 ng mL^{-1} BMP4 (Reprocell, 03–0007), then transferred to new 96-well U-bottom plates in 100 μL of the same new differentiation media. On day 3 of differentiation, an additional 25 μL of E6n containing 250 ng/mL FGF-2, 200 nM LDN-193189 (Stemgent, 04–0074-02) was added to each well (125 μL total media/well). Culture medium was changed completely on days 7 and 9 by washing as before, 3 times with DMEM:F12+HEPES and 3 times with E6n containing 3 μM CHIR 99021 (Reprocell, 04–0004-10), 200 nM LDN, and 50 ng/mL FGF-2, then transferred to new 96-well U-bottom plates in 250 uL of new media. On day 11, aggregates were washed as before, then 10 aggregates per well were transferred to a Nunc Delta surface 6-well culture dish in Organoid Maturation Medium (OMM) containing 1% GFR Matrigel and 3 μM CHIR99021. OMM consists of a 50:50 mixture of Advanced DMEM:F12 (Thermo Fisher, 12634028) and Neurobasal Medium (Thermo Fisher, 21103049) supplemented with 0.5× N2 Supplement (Thermo Fisher, 17502048), 0.5× B27 minus Vitamin A (Thermo Fisher, 12587010), 1× GlutaMAX (Thermo Fisher, 35050061), 0.1 mM β-Mercaptoethanol (Thermo Fisher, 21985023), and Normocin. Until day 13, CTRL and cochlear cultures received identical treatment. Day 13 cultures were split into CTRL or cochlear as follows: CTRL cultures were maintained in OMM + 3 μM CHIR99021 until day 18 with media changes on days 13 and 15 (to refresh media, washes are not necessary as the composition of the media does not change). On day 18, CTRL cultures were washed and transferred to a 10 cm culture dish in OMM (NO CHIR99021) and received twice-weekly media changes using fresh OMM for the remainder of the culture. On day 13 and 15, PUR+IWP2 culture media was changed to OMM + 3 μM CHIR99021 + 1 μM Purmorphamine (Stemgent, 04–0009). On day 18, PUR+IWP2 aggregates were washed to remove CHIR99021, and the media was changed to OMM + 3 μM IWP-2 (Tocris, 3533) +1 μM Purmorphamine. The media was changed on day 20 with fresh identical media. On day 22, PUR+IWP2 cultures were washed and transferred to a 10 cm culture dish in OMM-only, and received twice-weekly media changes using fresh OMM for the remainder of the culture.

Immunohistochemistry—Aggregates were fixed with 4% paraformaldehyde for 30 min at room temperature or at 4 °C overnight. The fixed specimens were cryoprotected with a

graded series of sucrose and then embedded in tissue-freezing medium. Frozen tissue blocks were sectioned into 12-μm cryosections on a Leica CM-1860 cryostat. For immunostaining, a 10% goat or horse serum in 0.1% Triton X-100 1× PBS solution was used for blocking, and a 3% goat or horse serum in 0.1–1% Triton X-100 1× PBS solution was used for primary/secondary antibody incubations. Primary antibodies used in this study are listed in Supplementary Table 1. Alexa Fluor conjugated antimouse, rabbit, or goat IgG (Thermo Fisher) were used as secondary antibodies. ProLong Gold Antifade Reagent with DAPI (Thermo Fisher) was used to mount the samples and visualize cellular nuclei.

For whole-mount immunofluorescence, the AbScale tissue-clearing protocol (Hama et al., 2015) was applied to aggregate samples. Incubation and washing steps were performed on a rotor, and incubation steps were performed at 37°C on a rotor unless otherwise noted. After fixation of samples with 4% paraformaldehyde overnight, the samples were incubated for 6 h in Scale S0 solution, followed by incubation in Scale A2 for 16 h, ScaleB4 solution for 24 h, and ScaleA2 solution for 8 h. Thereafter the samples were incubated in 0.1M PBS for 4 h at room temperature, and blocking was performed with 10% normal horse serum (Vector Laboratories) in AbScale solution for 16 h. Incubation with primary antibodies in AbScale solution containing 3% normal horse serum was performed for 48 h, followed by sequential washing with AbScale solution for 15, 30, 60, and 120 min and incubation with fluorophore-conjugated secondary antibodies in AbScale solution containing 3% normal horse serum for 24 h. After rinsing three times with AbScale at RT for 30 min and twice with AbScale Rinse solution at RT for 30 min, the samples were re-fixed with 4% paraformaldehyde at RT for 1 h, washed twice with 0.1M PBS, and incubated in ScaleS4 solution for 16 h. The stained samples were mounted with a small amount of ScaleS4 solution on poly-L-ornithine coated coverslips with silicone gaskets (Fisher Scientific). Imaging of the samples was carried out on a Leica Dive Confocal/Multiphoton Microscope or a Nikon A1R HD25 confocal microscope. Three-dimensional reconstructions were performed using the Imaris 8 software package (Bitplane) and the NIS Elements Advanced Research application (Nikon).

Quantification of immunohistochemistry data—Treated and control samples were processed for immunostaining simultaneously using identical reagents and protocols for each comparison. Images were acquired using either a Nikon A1R-HD25 confocal microscope, or a Leica DMI8 widefield fluorescent microscope using identical image acquisition parameters between conditions. Raw images were analysed using Nikon GI3 suite or exported in TIFF format and analysed using ImageJ[59]. Co-expression analysis was performed by analysing regions for coincident signal corresponding to a labelled tissue-specific marker and a gene of interest. Mean grey value and total colocalized area were collected. Statistical analysis was performed in GraphPad Prism 9.

Scanning electron microscopy—Aggregates with abundant *POU4F3*-ntdTomato+ puncta between D81 and 141 of differentiation were fixed with 2.5% glutaraldehyde in sodium cacodylate buffer (Electron Microscopy Sciences) at 4°C overnight. The fixed samples were dissected under a Nikon SMZ18 stereo fluorescence microscope to expose the luminal surface of vesicles containing ntdTomato+ cells and post-fixed with 1% osmium tetroxide (Electron Microscopy Sciences) at RT for 1 h. The samples were then dehydrated

through a graded series of ethanol and transferred into a Leica EM CPD300 critical-point dryer. After critical point drying, the samples were mounted on aluminium stubs and sputter coated with a Denton Vacuum Desk V sample preparation system. The samples were viewed on a JEOL JSM-7800F field emission scanning electron microscope at an accelerating voltage of 5 kV.

Representative data and reproducibility—Unless stated otherwise, images are representative of specimens obtained from at least three separate experiments. For immunohistochemical analysis of aggregates, we typically sectioned 6–15 aggregates from each condition in each experiment.

scRNA-seq and raw data processing—*PAX2*^{nG}+ (D20 samples) or *POU4F3*^{nT}+ (D80 and −109 samples) cells were isolated and used for scRNA-seq analyses. Thirty to 45 aggregates per condition were washed with 0.5 mM EDTA (Thermo Fisher) in DPBS, then incubated with 1.1 mM EDTA in 1X TrypLE (Life Technologies) in DPBS on an orbital shaker at 37°C for 30 min followed by 40–50 min without shaking. During incubation, the samples were mechanically dissociated on Nunclon Sphera 24-well plates (Thermo Fisher) with shaking and occasional gentle pipetting with P1000 tips. After confirming that most cells, especially those with reporter expression, were completely dissociated, they were filtered sequentially through a 100-μm and a 40-μm cell strainer (Falcon) and then transferred into 2-ml tubes (Eppendorf). After spinning down at 100 × *g* for 5 min, dissociated cells were resuspended in FACS buffer consisting of 2% fetal bovine serum (Thermo Fisher) in 1X DPBS. Cells were again filtered through a 40-μm cell strainer and collected into a 5-ml round-bottom polypropylene tube (Falcon). Dead cells were stained with propidium iodide (PI, Invitrogen) diluted at 1:500. Simultaneously, size control cells without PI staining were prepared using aggregates made from wild-type hESCs using the above protocol. Cells were stored on ice and protected from light prior to sorting. PI-negative and GFP (or tdTomato)-positive populations were collected and cleaned using a SORP Aria (BD Biosciences).

For collecting EPCAM-positive and -negative cells, dissociated D81 organoid cells were stained with 1:100 PE-conjugated EPCAM antibody (BioLegend) for 40 min prior to FACS sorting. PE-EPCAM^{+} and PE-EPCAM^{-} populations were collected in separate tubes for separate downstream scNA-seq reactions. Since *POU4F3*$^{nT+}$ hair cells also express EPCAM on their cell surfaces, these hair cells exhibit both tdTomato and PE fluorescence signals, both of which are red. As a result, hair cells were FACS-isolated as a sub-population of PE-EPCAM^{+} cells.

scRNA-seq for all samples was performed using the 10X Genomics Chromium 3’ v3 platform for cDNA library construction and the NovaSeq 6000 system (Illumina) for sequencing. For each sample, between 12,000 and 18,000 cells were added to the single cell master mix, following the Chromium NextGEM Single Cell 3’ Reagent Kits User Guide. The single cell master mix, along with the single-cell gel beads and partitioning oil, was dispensed onto a Single Cell Chip G and the chip was loaded into the Chromium Controller for barcoding and cDNA synthesis. The resulting cDNA library was sequenced

with the NovaSeq 6000 system running a custom program for 28-bp plus 91-bp paired-end sequencing, resulting in a read depth of more than 40,000 reads per cell.

Illumina's CellRanger v4.0.0 program was used to generate BCL files, which were demutiplexed and converted to FASTQ files via bcl2fastq Conversion Software (Illumina). The FASTQ files were then aligned to the GRCh38–3.0.0 reference genome using the STAR (Spliced Transcripts Alignment to a Reference) aligner. Mapped reads were grouped by cell barcode, single-cell gene expression was quantified using unique molecular identifiers (UMIs), and the resulting filtered gene-barcode (count) matrices were used as input for downstream analysis.

scRNA-seq data analysis—The filtered count matrices were preprocessed individually for each dataset, removing cells where the number of mitochondrial gene counts exceeded 12.5 percent of the total number of molecules detected. A second preprocessing step removed cells with anomalous housekeeping gene expression: Cells with log-transformed RPL27 expression ± 2 standard deviations away from the mean were removed. After preprocessing, datasets were merged across conditions, resulting in one combined dataset for each timepoint. After merging, the gene expression levels were normalized using the SCTransform function in Seurat [60], which transforms raw count data into Pearson residuals, effectively controlling for technical variation resulting from heterogenous sequencing depth. Over fifty different cluster partitions were generated using Seurat's unsupervised clustering workflow by varying the values of the resolution and k.param parameters required for clustering and shared nearest neighbor graph construction, respectively. Then, the cluster partition with the highest silhouette index was selected for further analysis [61]. Cluster identity was manually determined based on the expression of canonical markers.

Relevant populations (e.g. otic progenitors, hair cells) were isolated on the basis of cluster identity and comparisons between treatment groups were performed using DESeq2 and zingeR [62]. Cell-level weights – which are required to adjust for drop-out events endemic to scRNA-sequencing – were calculated with zingeR. Differential expression between treatment groups was determined using DESeq2, and genes were considered statistically significant with a Benjamini-Hochberg $P < 0.05$. The results of the DESeq2 analysis were passed to iDEA [21], a platform for gene set enrichment analysis, and differentially expressed genes were compared to gene sets taken from MSigDB databases [63]. The Gene Transcription Regulation Database (GTRD) was used to define the 573 transcription factor target gene sets our data were compared against [64]. While these gene sets are well defined, they do not constitute an exhaustive list of all possible transcription factors.

Electrophysiological analyses—D138–164 hESC-derived organoids were first imaged in bright field and epifluorescent illumination (TE2000-U, Nikon) to determine localization of otic vesicles with tdTomato positive cells. Then, the organoids were sectioned with a diamond knife to expose otic vesicles. The section was placed into the custom-made recording chamber, where it was held by two strands of dental floss. The recordings were performed at room temperature (20–25°C) in Leibovitz's L-15 cell culture medium (Cat #21083027, Gibco/ThermoFisher, USA) containing the following inorganic salts (in mM): NaCl (137), KCl (5.4), CaCl2 (1.26), MgCl2 (1.0), Na2HPO4 (1.0), KH2PO4 (0.44),

MgSO4 (0.81). The cells were viewed with an upright microscope (E600FN, Nikon), equipped with a high numerical aperture (NA) objective (60x, 1.0 NA) and epifluoresent attachment. Only the cells with bright tdTomato signal were chosen for recordings. During recordings, the organoid sections were continuously perfused with L-15 medium. Pipettes for whole-cell patch-clamp recordings were filled with intracellular solution containing (in mM): KCl(12.6), KGlu(131.4), MgCl2(2), EGTA(0.5), K2HPO4 (8), KH2PO4 (2), Mg2-ATP (2), and Na4-GTP(0.2). The solution was adjusted to pH 7.3–7.4 with KOH and to 320 mOsm with D-glucose. The uncompensated pipette resistance was typically 5–8 MOhm when measured in the bath. Whole cell current responses were recorded with a MultiClamp 700B patch clamp amplifier controlled by pClamp software (Molecular Devices, USA).

Human tissue ethics, collection and immunofluorescence—Human fetal cochleae were collected and processed at the Leiden University Medical Center (Netherland) from tissues obtained from elective abortion using vacuum aspiration. Prior to the procedure, obstetric ultrasonography was performed to determine the gestational weeks (GW) and days. One GW 13 cochlear, one GW18 cochlear and one GW 18 vestibular samples were used in this study. The fresh samples were collected in PBS, fixed in 4% paraformaldehyde in PBS overnight at 4°C, decalcified and embedded in paraffin as previously described [65]. The paraffin blocks were cut into 5 μm thick sections through the sagittal plane using a Leica rotary microtome. The serial sections were deparaffinized in xylene, rehydrated in a descending ethanol series (100%, 90%, 70%, 50%), and rinsed in distilled water. Thereafter, the sections were treated in 0.01 M sodium citrate buffer (pH 6.0) for 12 minutes at 98 °C using a boiling pot for antigen-retrieval and then processed for immunofluorescence. Primary antibodies used in this study are listed in Supplementary Table 1. The stained samples were viewed and imaged on a Zeiss LSM900 confocal microscope. The use of human fetal tissues was approved by the Medical Ethical Committee of the Leiden University Medical Center (Protocol Number 08.087). Informed written consents were obtained in accordance with the WMA Declaration of Helsinki guidelines.

QUANTIFICATION AND STATISTICAL ANALYSIS

Data are presented as mean ± SEM and were derived from at least 3 independent experiments unless otherwise indicated. Statistical analysis was carried out in Graphpad Prism 9. Paired analyses were performed using a two-sided Welch’s t-test. Multiple comparisons were performed using one-way ANOVA with Tukey’s multiple comparisons test. For both tests the cutoff for statistical significance was $P<0.01$. Information regarding replicates (n), definition of center, statistical tests, and significance notation can be found in the figure legends.

Supplementary Material

Refer to Web version on PubMed Central for supplementary material.

ACKNOWLEDGEMENTS

This work was supported by a Department of Defense U.S. Army Medical Research and Materiel Command Congressionally Directed Medical Research Program grant W81XWH-18-1-0062 (E. H.), National Institute of Health grants R01 DC013294 and R01 DC015788 (E.H.), K08 DC016034 (R.F.N.), JSPS KAKENHI Grant

Number JP21K09638 (T.N.), the Indiana University Health-Indiana University School of Medicine Strategic Research Initiative (E.H.), and the Ruth C. Holton Research Funds (E.H.). The authors would like to thank the Center for Contraception, Sexuality and Abortion (CASA) in Leiden and The Hague for the collection of the human fetal material, B. Daye, T. van der Helm, F. Wei, J. Harkin, T. Saeki, M. Jafarkkhani, E. Longworth-Mills, P. McGuire, H. Gao for their expert technical assistance, J. Zheng, K. Homma for antibodies against PRESTIN, and M. W. Kelley for his comments on the manuscript.

INCLUSION AND DIVERSITY

We support inclusive, diverse, and equitable conduct of research.

REFRENCES

1. Barald KF, and Kelley MW (2004). From placode to polarization: new tunes in inner ear development. Development 131, 4119–4130. 10.1242/dev.01339. [PubMed: 15319325]
2. Groves AK, and Fekete DM (2012). Shaping sound in space: the regulation of inner ear patterning. Development 139, 245–257. 10.1242/dev.067074. [PubMed: 22186725]
3. Wu DK, and Kelley MW (2012). Molecular mechanisms of inner ear development. Cold Spring Harb Perspect Biol 4, a008409. 10.1101/cshperspect.a008409. [PubMed: 22855724]
4. Morton CC, and Nance WE (2006). Newborn hearing screening--a silent revolution. N Engl J Med 354, 2151–2164. 10.1056/NEJMra050700. [PubMed: 16707752]
5. Koehler KR, Mikosz AM, Molosh AI, Patel D, and Hashino E (2013). Generation of inner ear sensory epithelia from pluripotent stem cells in 3D culture. Nature 500, 217–221. 10.1038/nature12298. [PubMed: 23842490]
6. Koehler KR, and Hashino E (2014). 3D mouse embryonic stem cell culture for generating inner ear organoids. Nat Protoc 9, 1229–1244. 10.1038/nprot.2014.100. [PubMed: 24784820]
7. Liu XP, Koehler KR, Mikosz AM, Hashino E, and Holt JR (2016). Functional development of mechanosensitive hair cells in stem cell-derived organoids parallels native vestibular hair cells. Nat Commun 7, 11508. 10.1038/ncomms11508. [PubMed: 27215798]
8. Koehler KR, Nie J, Longworth-Mills E, Liu XP, Lee J, Holt JR, and Hashino E (2017). Generation of inner ear organoids containing functional hair cells from human pluripotent stem cells. Nat Biotechnol 35, 583–589. 10.1038/nbt.3840. [PubMed: 28459451]
9. Nie J, Ueda Y, Solivais AJ, and Hashino E (2022). CHD7 regulates otic lineage specification and hair cell differentiation in human inner ear organoids. Nat Commun 13, 7053. 10.1038/s41467-022-34759-8. [PubMed: 36396635]
10. Jeong M, O'Reilly M, Kirkwood NK, Al-Aama J, Lako M, Kros CJ, and Armstrong L (2018). Generating inner ear organoids containing putative cochlear hair cells from human pluripotent stem cells. Cell Death Dis 9, 922. 10.1038/s41419-018-0967-1. [PubMed: 30206231]
11. Bouchard M, de Caprona D, Busslinger M, Xu P, and Fritzsch B (2010). Pax2 and Pax8 cooperate in mouse inner ear morphogenesis and innervation. BMC Dev Biol 10, 89. 10.1186/1471-213X-10-89. [PubMed: 20727173]
12. Xiang M, Gan L, Li D, Chen ZY, Zhou L, O'Malley BW Jr., Klein W, and Nathans J (1997). Essential role of POU-domain factor Brn-3c in auditory and vestibular hair cell development. Proc Natl Acad Sci U S A 94, 9445–9450. 10.1073/pnas.94.17.9445. [PubMed: 9256502]
13. Hertzano R, Montcouquiol M, Rashi-Elkeles S, Elkon R, Yucel R, Frankel WN, Rechavi G, Moroy T, Friedman TB, Kelley MW, and Avraham KB (2004). Transcription profiling of inner ears from Pou4f3(ddl/ddl) identifies Gfi1 as a target of the Pou4f3 deafness gene. Hum Mol Genet 13, 2143–2153. 10.1093/hmg/ddh218. [PubMed: 15254021]
14. Kleinstiver BP, Pattanayak V, Prew MS, Tsai SQ, Nguyen NT, Zheng Z, and Joung JK (2016). High-fidelity CRISPR-Cas9 nucleases with no detectable genome-wide off-target effects. Nature 529, 490–495. 10.1038/nature16526. [PubMed: 26735016]
15. Nie J, and Hashino E (2020). Generation of inner ear organoids from human pluripotent stem cells. Methods Cell Biol 159, 303–321. 10.1016/bs.mcb.2020.02.006. [PubMed: 32586448]

16. Ueda Y, Moore ST, and Hashino E (2022). Directed Differentiation of Human Pluripotent Stem Cells into Inner Ear Organoids. Methods Mol Biol 2520, 135–150. 10.1007/7651_2021_448. [PubMed: 34724191]
17. Riccomagno MM, Martinu L, Mulheisen M, Wu DK, and Epstein DJ (2002). Specification of the mammalian cochlea is dependent on Sonic hedgehog. Genes Dev 16, 2365–2378. 10.1101/gad.1013302. [PubMed: 12231626]
18. Ohta S, Wang B, Mansour SL, and Schoenwolf GC (2016). SHH ventralizes the otocyst by maintaining basal PKA activity and regulating GLI3 signaling. Dev Biol 420, 100–109. 10.1016/j.ydbio.2016.10.004. [PubMed: 27720745]
19. Riccomagno MM, Takada S, and Epstein DJ (2005). Wnt-dependent regulation of inner ear morphogenesis is balanced by the opposing and supporting roles of Shh. Genes Dev 19, 1612–1623. 10.1101/gad.1303905. [PubMed: 15961523]
20. Ohta S, Wang B, Mansour SL, and Schoenwolf GC (2016). BMP regulates regional gene expression in the dorsal otocyst through canonical and non-canonical intracellular pathways. Development 143, 2228–2237. 10.1242/dev.137133. [PubMed: 27151948]
21. Ma Y, Sun S, Shang X, Keller ET, Chen M, and Zhou X (2020). Integrative differential expression and gene set enrichment analysis using summary statistics for scRNA-seq studies. Nat Commun 11, 1585. 10.1038/s41467-020-15298-6. [PubMed: 32221292]
22. Burns JC, Kelly MC, Hoa M, Morell RJ, and Kelley MW (2015). Single-cell RNA-Seq resolves cellular complexity in sensory organs from the neonatal inner ear. Nat Commun 6, 8557. 10.1038/ncomms9557. [PubMed: 26469390]
23. Kolla L, Kelly MC, Mann ZF, Anaya-Rocha A, Ellis K, Lemons A, Palermo AT, So KS, Mays JC, Orvis J, et al. (2020). Characterization of the development of the mouse cochlear epithelium at the single cell level. Nat Commun 11, 2389. 10.1038/s41467-020-16113-y. [PubMed: 32404924]
24. Scheffer DI, Shen J, Corey DP, and Chen ZY (2015). Gene Expression by Mouse Inner Ear Hair Cells during Development. J Neurosci 35, 6366–6380. 10.1523/jneurosci.5126-14.2015. [PubMed: 25904789]
25. Elkon R, Milon B, Morrison L, Shah M, Vijayakumar S, Racherla M, Leitch CC, Silipino L, Hadi S, Weiss-Gayet M, et al. (2015). RFX transcription factors are essential for hearing in mice. Nat Commun 6, 8549. 10.1038/ncomms9549. [PubMed: 26469318]
26. Barr-Gillespie PG (2015). Assembly of hair bundles, an amazing problem for cell biology. Mol Biol Cell 26, 2727–2732. 10.1091/mbc.E14-04-0940. [PubMed: 26229154]
27. Zheng J, Shen W, He DZ, Long KB, Madison LD, and Dallos P (2000). Prestin is the motor protein of cochlear outer hair cells. Nature 405, 149–155. 10.1038/35012009. [PubMed: 10821263]
28. Homma K, Miller KK, Anderson CT, Sengupta S, Du GG, Aguinaga S, Cheatham M, Dallos P, and Zheng J (2010). Interaction between CFTR and prestin (SLC26A5). Biochim Biophys Acta 1798, 1029–1040. 10.1016/j.bbamem.2010.02.001. [PubMed: 20138822]
29. Kros CJ, Ruppersberg JP, and Rusch A (1998). Expression of a potassium current in inner hair cells during development of hearing in mice. Nature 394, 281–284. 10.1038/28401. [PubMed: 9685158]
30. Marcotti W, and Kros CJ (1999). Developmental expression of the potassium current IK,n contributes to maturation of mouse outer hair cells. J Physiol 520 Pt 3, 653–660. 10.1111/j.1469-7793.1999.00653.x. [PubMed: 10545133]
31. Gow A, Davies C, Southwood CM, Frolenkov G, Chrustowski M, Ng L, Yamauchi D, Marcus DC, and Kachar B (2004). Deafness in Claudin 11-null mice reveals the critical contribution of basal cell tight junctions to stria vascularis function. J Neurosci 24, 7051–7062. 10.1523/jneurosci.1640-04.2004. [PubMed: 15306639]
32. Korrapati S, Taukulis I, Olszewski R, Pyle M, Gu S, Singh R, Griffiths C, Martin D, Boger E, Morell RJ, and Hoa M (2019). Single Cell and Single Nucleus RNA-Seq Reveal Cellular Heterogeneity and Homeostatic Regulatory Networks in Adult Mouse Stria Vascularis. Front Mol Neurosci 12, 316. 10.3389/fnmol.2019.00316. [PubMed: 31920542]
33. Nichols DH, Pauley S, Jahan I, Beisel KW, Millen KJ, and Fritzsch B (2008). Lmx1a is required for segregation of sensory epithelia and normal ear histogenesis and morphogenesis. Cell Tissue Res 334, 339–358. 10.1007/s00441-008-0709-2. [PubMed: 18985389]

34. Koo SK, Hill JK, Hwang CH, Lin ZS, Millen KJ, and Wu DK (2009). Lmx1a maintains proper neurogenic, sensory, and non-sensory domains in the mammalian inner ear. Dev Biol 333, 14–25. 10.1016/j.ydbio.2009.06.016. [PubMed: 19540218]
35. Luo XJ, Deng M, Xie X, Huang L, Wang H, Jiang L, Liang G, Hu F, Tieu R, Chen R, and Gan L (2013). GATA3 controls the specification of prosensory domain and neuronal survival in the mouse cochlea. Hum Mol Genet 22, 3609–3623. 10.1093/hmg/ddt212. [PubMed: 23666531]
36. Bardhan T, Jeng JY, Waldmann M, Ceriani F, Johnson SL, Olt J, Rüttiger L, Marcotti W, and Holley MC (2019). Gata3 is required for the functional maturation of inner hair cells and their innervation in the mouse cochlea. J Physiol 597, 3389–3406. 10.1113/jp277997. [PubMed: 31069810]
37. Karis A, Pata I, van Doorninck JH, Grosveld F, de Zeeuw CI, de Caprona D, and Fritzsch B (2001). Transcription factor GATA-3 alters pathway selection of olivocochlear neurons and affects morphogenesis of the ear. J Comp Neurol 429, 615–630. 10.1002/1096-9861(20010122)429:4<615::aid-cne8>3.0.co;2-f. [PubMed: 11135239]
38. Tang LS, Alger HM, and Pereira FA (2006). COUP-TFI controls Notch regulation of hair cell and support cell differentiation. Development 133, 3683–3693. 10.1242/dev.02536. [PubMed: 16914494]
39. Tang K, Xie X, Park JI, Jamrich M, Tsai S, and Tsai MJ (2010). COUP-TFs regulate eye development by controlling factors essential for optic vesicle morphogenesis. Development 137, 725–734. 10.1242/dev.040568. [PubMed: 20147377]
40. McInturff S, Burns JC, and Kelley MW (2018). Characterization of spatial and temporal development of Type I and Type II hair cells in the mouse utricle using new cell-type-specific markers. Biol Open 7. 10.1242/bio.038083.
41. Driver EC, and Kelley MW (2020). Development of the cochlea. Development 147. 10.1242/dev.162263.
42. Thulasiram MR, Ogier JM, and Dabdoub A (2022). Hearing Function, Degeneration, and Disease: Spotlight on the Stria Vascularis. Front Cell Dev Biol 10, 841708. 10.3389/fcell.2022.841708.
43. Kelly MC, and Chen P (2009). Development of form and function in the mammalian cochlea. Curr Opin Neurobiol 19, 395–401. 10.1016/j.conb.2009.07.010. [PubMed: 19683914]
44. Brigande JV, Kiernan AE, Gao X, Iten LE, and Fekete DM (2000). Molecular genetics of pattern formation in the inner ear: do compartment boundaries play a role? Proc Natl Acad Sci U S A 97, 11700–11706. 10.1073/pnas.97.22.11700. [PubMed: 11050198]
45. Kil SH, and Collazo A (2002). A review of inner ear fate maps and cell lineage studies. J Neurobiol 53, 129–142. 10.1002/neu.10127. [PubMed: 12382271]
46. Vélez-Ortega AC, Freeman MJ, Indzhykulian AA, Grossheim JM, and Frolenkov GI (2017). Mechanotransduction current is essential for stability of the transducing stereocilia in mammalian auditory hair cells. Elife 6. 10.7554/eLife.24661.
47. Hadi S, Alexander AJ, Vélez-Ortega AC, and Frolenkov GI (2020). Myosin-XVa Controls Both Staircase Architecture and Diameter Gradation of Stereocilia Rows in the Auditory Hair Cell Bundles. J Assoc Res Otolaryngol 21, 121–135. 10.1007/s10162-020-00745-4. [PubMed: 32152769]
48. Wiwatpanit T, Lorenzen SM, Cantú JA, Foo CZ, Hogan AK, Márquez F, Clancy JC, Schipma MJ, Cheatham MA, Duggan A, and García-Añoveros J (2018). Trans-differentiation of outer hair cells into inner hair cells in the absence of INSM1. Nature 563, 691–695. 10.1038/s41586-018-0570-8. [PubMed: 30305733]
49. García-Añoveros J, Clancy JC, Foo CZ, García-Gómez I, Zhou Y, Homma K, Cheatham MA, and Duggan A (2022). Tbx2 is a master regulator of inner versus outer hair cell differentiation. Nature 605, 298–303. 10.1038/s41586-022-04668-3. [PubMed: 35508658]
50. Dressler GR, and Douglass EC (1992). Pax-2 is a DNA-binding protein expressed in embryonic kidney and Wilms tumor. Proc Natl Acad Sci U S A 89, 1179–1183. 10.1073/pnas.89.4.1179. [PubMed: 1311084]
51. Tavassoli K, Rüger W, and Horst J (1997). Alternative splicing in PAX2 generates a new reading frame and an extended conserved coding region at the carboxy terminus. Hum Genet 101, 371–375. 10.1007/s004390050644. [PubMed: 9439670]

52. Ward TA, Nebel A, Reeve AE, and Eccles MR (1994). Alternative messenger RNA forms and open reading frames within an additional conserved region of the human PAX-2 gene. Cell Growth Differ 5, 1015–1021. [PubMed: 7819127]
53. Gibson DG, Young L, Chuang RY, Venter JC, Hutchison CA 3rd, and Smith HO (2009). Enzymatic assembly of DNA molecules up to several hundred kilobases. Nat Methods 6, 343–345. 10.1038/nmeth.1318. [PubMed: 19363495]
54. Hockemeyer D, Wang H, Kiani S, Lai CS, Gao Q, Cassady JP, Cost GJ, Zhang L, Santiago Y, Miller JC, et al. (2011). Genetic engineering of human pluripotent cells using TALE nucleases. Nat Biotechnol 29, 731–734. 10.1038/nbt.1927. [PubMed: 21738127]
55. Slaymaker IM, Gao L, Zetsche B, Scott DA, Yan WX, and Zhang F (2016). Rationally engineered Cas9 nucleases with improved specificity. Science 351, 84–88. 10.1126/science.aad5227. [PubMed: 26628643]
56. Maruyama T, Dougan SK, Truttmann MC, Bilate AM, Ingram JR, and Ploegh HL (2015). Increasing the efficiency of precise genome editing with CRISPR-Cas9 by inhibition of nonhomologous end joining. Nat Biotechnol 33, 538–542. 10.1038/nbt.3190. [PubMed: 25798939]
57. Matsuda T, and Cepko CL (2007). Controlled expression of transgenes introduced by in vivo electroporation. Proc Natl Acad Sci U S A 104, 1027–1032. 10.1073/pnas.0610155104. [PubMed: 17209010]
58. Raymond CS, and Soriano P (2007). High-efficiency FLP and PhiC31 site-specific recombination in mammalian cells. PLoS One 2, e162. 10.1371/journal.pone.0000162. [PubMed: 17225864]
59. Schneider CA, Rasband WS, and Eliceiri KW (2012). NIH Image to ImageJ: 25 years of image analysis. Nat Methods 9, 671–675. 10.1038/nmeth.2089. [PubMed: 22930834]
60. Hao Y, Hao S, Andersen-Nissen E, Mauck WM 3rd, Zheng S, Butler A, Lee MJ, Wilk AJ, Darby C, Zager M, et al. (2021). Integrated analysis of multimodal single-cell data. Cell 184, 3573–3587.e3529. 10.1016/j.cell.2021.04.048. [PubMed: 34062119]
61. Rousseeuw PJ (1987). Silhouettes - a Graphical Aid to the Interpretation and Validation of Cluster-Analysis. J Comput Appl Math 20, 53–65. doi:Doi 10.1016/0377-0427(87)90125-7 (1987).
62. Love MI, Huber W, and Anders S (2014). Moderated estimation of fold change and dispersion for RNA-seq data with DESeq2. Genome Biol 15, 550. 10.1186/s13059-014-0550-8. [PubMed: 25516281]
63. Subramanian A, Tamayo P, Mootha VK, Mukherjee S, Ebert BL, Gillette MA, Paulovich A, Pomeroy SL, Golub TR, Lander ES, and Mesirov JP (2005). Gene set enrichment analysis: a knowledge-based approach for interpreting genome-wide expression profiles. Proc Natl Acad Sci U S A 102, 15545–15550. 10.1073/pnas.0506580102. [PubMed: 16199517]
64. Kolmykov S, Yevshin I, Kulyashov M, Sharipov R, Kondrakhin Y, Makeev VJ, Kulakovskiy IV, Kel A, and Kolpakov F (2021). GTRD: an integrated view of transcription regulation. Nucleic Acids Res 49, D104–d111. 10.1093/nar/gkaa1057. [PubMed: 33231677]
65. Locher H, Frijns JH, van Iperen L, de Groot JC, Huisman MA, and Chuva de Sousa Lopes SM (2013). Neurosensory development and cell fate determination in the human cochlea. Neural Dev 8, 20. 10.1186/1749-8104-8-20. [PubMed: 24131517]

Highlights

- Timed modulations of SHH and WNT ventralize hPSC-derived inner ear organoids
- Cochlear organoids exhibit highly differential expression of GATA3 and NR2F1
- Derived hair cells exhibit cochlear-like structural and functional properties
- Cochlear organoids give rise to both inner and outer hair cell-like cells

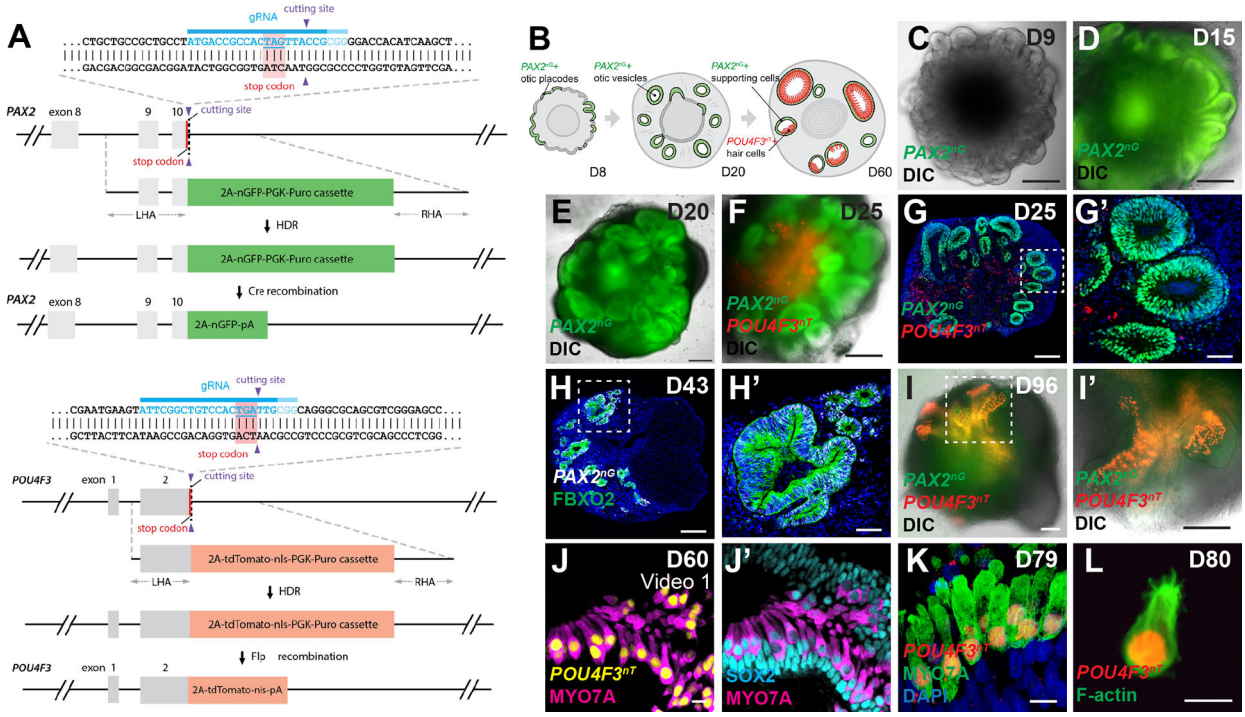

Figure 1. *PAX2*-2A-nGFP/*POU4F3*-2A-ntTomato (*PAX2*^{nG}/*POU4F3*^{nT}) multiplex reporter hESCs faithfully recapitulate otic progenitor and hair cell differentiations in inner ear organoids.

(A) Schematic illustrations of the *PAX2*-2A-nGFP and *POU4F3*-2A-ntdTomato CRISPR design.

(B) Schematic of *PAX2*^{nG} and *POU4F3*^{nT} reporter expression during inner ear organoid development.

(C-F) Live images of whole aggregates containing multiple developing inner ear organoids show the spatio-temporal progression of *PAX2*^{nG} reporter expression and early morphogenesis of *PAX2*+ epithelium.

(G-H) Representative images of hESC-derived aggregates showing *PAX2*^{nG}+ epithelium organized into vesicles that co-express the otic-specific marker FBXO2, but devoid of *POU4F3*^{nT} expression.

(I-I') Live images of late-stage (D96) aggregates showing intense *POU4F3*^{nT}+ puncta localized to epithelial vesicles.

(J-K) *POU4F3*^{nT}+ cells in inner ear organoids also express the hair cell markers MYO7A and SOX2, and are located on the luminal surface of SOX2+ supporting epithelia.

(L) Fixed cell suspension of dissociated *POU4F3*^{nT}+ cells isolated from D80 inner ear organoids reveals tdTomato+ nuclei and F-actin+ membranes and stereocilia.

Scale bars, 200 μm (C-G, H, I, I'), 50 μm (G', H'), 10 μm (J-L).

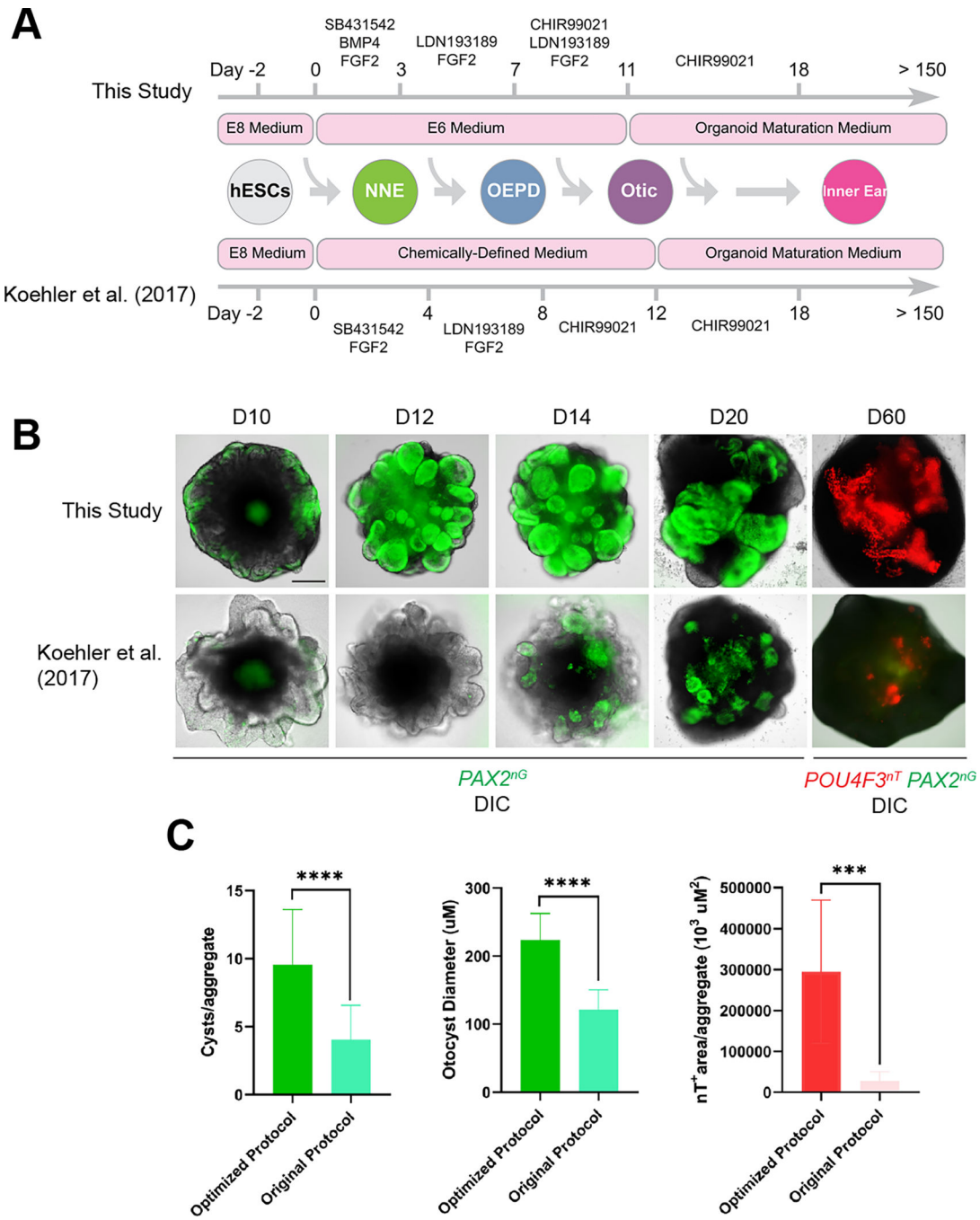

Figure 2. Optimization of inner ear organoid derivation protocol.

(A) Schematic comparison of our original vs. optimized protocol.

(B) Live images of whole cell aggregates containing inner ear organoids derived from our *PAX2*^{nG}/*POU4F3*^{nT} multiplex reporter hESC line cultured under the original vs. optimized protocol.

(C) Quantitative comparison of culture outcomes in optimized vs. original culture protocol on D60. n = 20 (green histograms), 13 (red histogram) biological samples from separate

experiments per group. Welch's two-sided *t*-test ***P=0.000132, ****P=0.000013 (#cysts) P<0.000001 (diameter).
Scale bars, 200 μm.

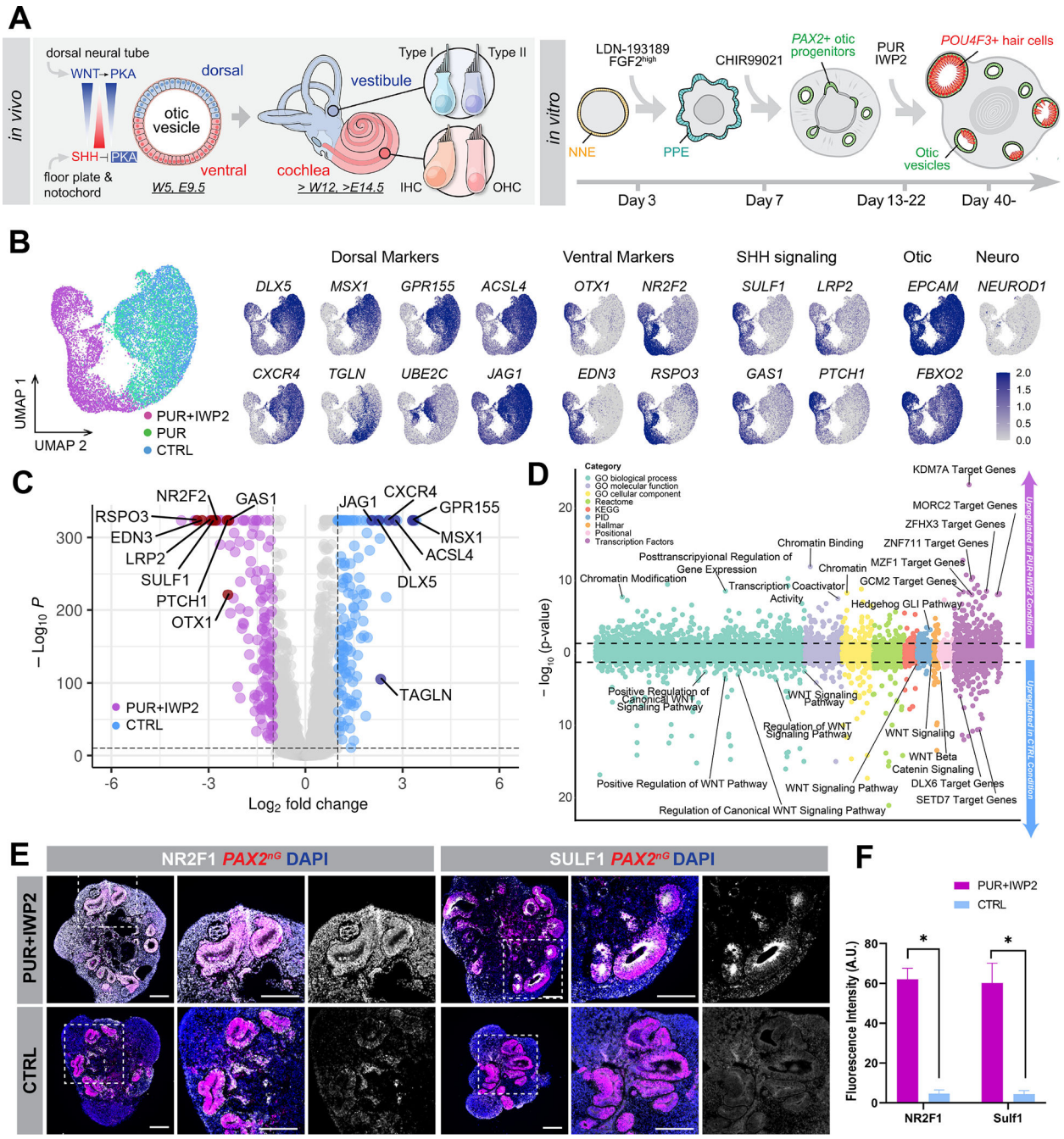

Figure 3. PUR+IWP2 treatment promotes ventralization of otic progenitors in human inner ear organoids.

(A) Schematic illustration of known ventralization and dorsalization signals during mouse inner ear development and application of this principle to the human inner ear organoid system. PKA: protein kinase A, W: human gestational week, E: mouse embryonic day. (B-D) D20 scRNA-seq analysis of FACS-sorted *PAX2*^{nG}+ otic progenitors in human inner ear organoids. UMAP projections of otic progenitors from PUR+IWP2, PUR and CTRL samples (B). Feature plots demonstrate that dorsal otic markers are predominantly expressed in PUR and CTRL otic progenitors, while ventral otic markers and SHH

signaling components are confined largely to PUR+IWP2 cells. Consistent with this, the volcano plot (C) shows differentially expressed dorsal and ventral otic marker genes between PUR+IWP2 and CTRL otic progenitors. Gene-set enrichment analysis of genes upregulated in the PUR+IWP2 and CTRL otic progenitors (above and below 0 in the bubble plot, respectively) (D) shows genes associated with posttranscriptional regulation of gene expression, chromatin modifications and Hedge Hog signaling are enriched in ventralized otic progenitors in inner ear organoids.

(E) Representative images of D25 samples show notably higher expression of NR2F1 and SUlF1 in PUR+IWP2 organoids vs. CTRL organoids.

(F) Quantitative analysis of vesicles co-expressing PAX2 and NR2F1 (or SULF1) in PUR+IWP2 vs. CTRL organoids; $n = 8$ biological samples from separate experiments per group; Welch's two-sided t-test $^{*}P=0.0013$ (NR2F1), $^{*}P=0.0089$ (SULF1); values are mean ± SEM.

Scale bars, 200 μm.

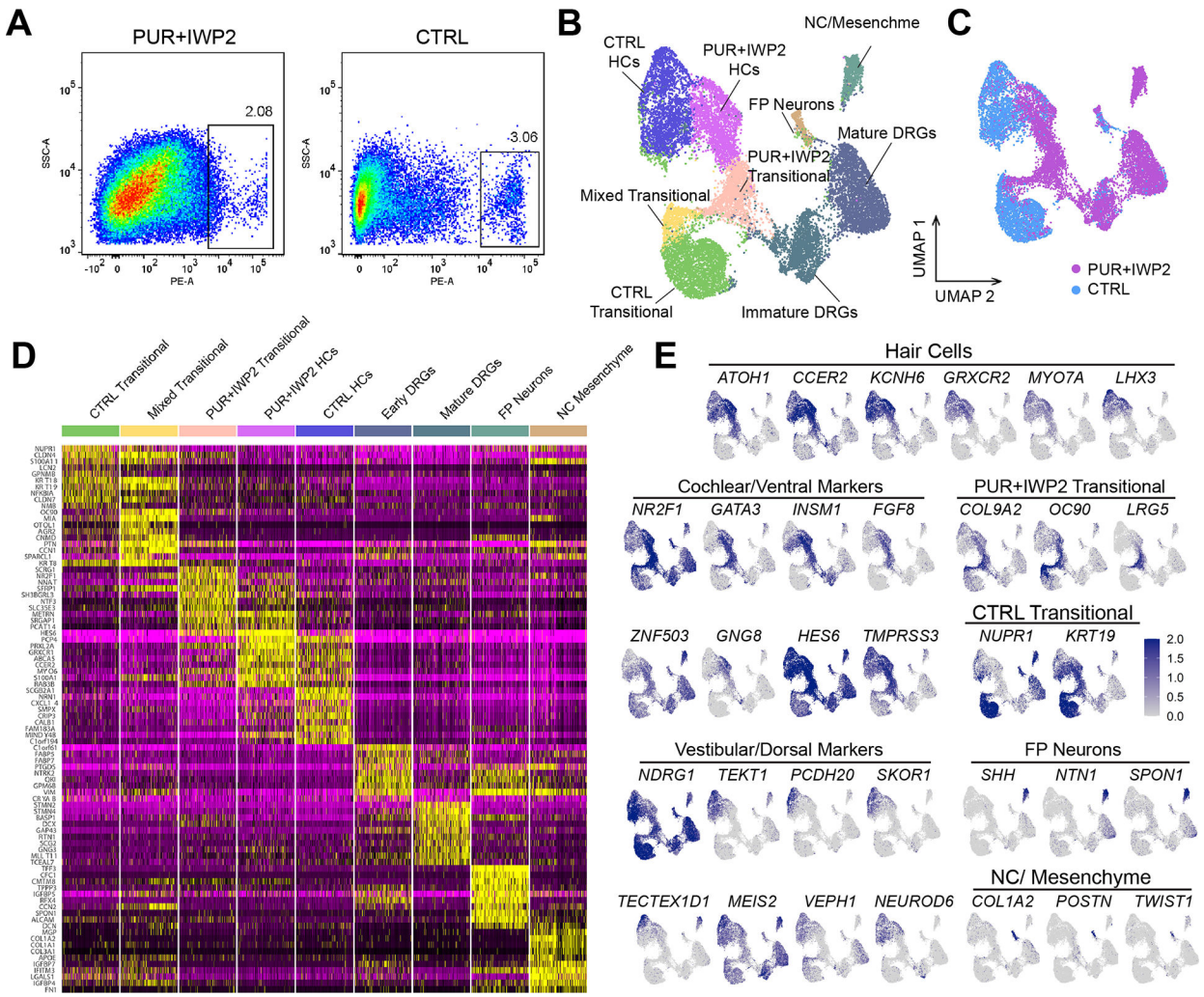

Figure 4. Differential gene expression in *POU4F3*^{nT}+ cells of D109 ventralized vs. control inner ear organoids.

(A) FACS gating strategy used to isolate *POU4F3*^{nT}+ cells from dissociated D109 inner ear organoids in PUR+IWP2 and CTRL conditions.

(B-C) UMAP plot of *POU4F3*^{nT}+ cells isolated from D109 PUR+IWP2 and CTRL inner ear organoids (B) and UMAP plot grouped by experimental conditions (C). The number of sequenced cells: 7,968 (CTRL), 11,107 (PUR+IWP2). The number of cells after QC filtering: 5,971 (CTRL), 10,073 (PUR-IWP2).

(D) Heat map showing gene expression across clusters.

(E) Feature plots showing the distributions of marker genes across the cluster map and those showing differential expression of known cochlear and vestibular marker genes in annotated hair cell populations.

DRG; dorsal root ganglion, FP; floor plate, NC; neural crest.

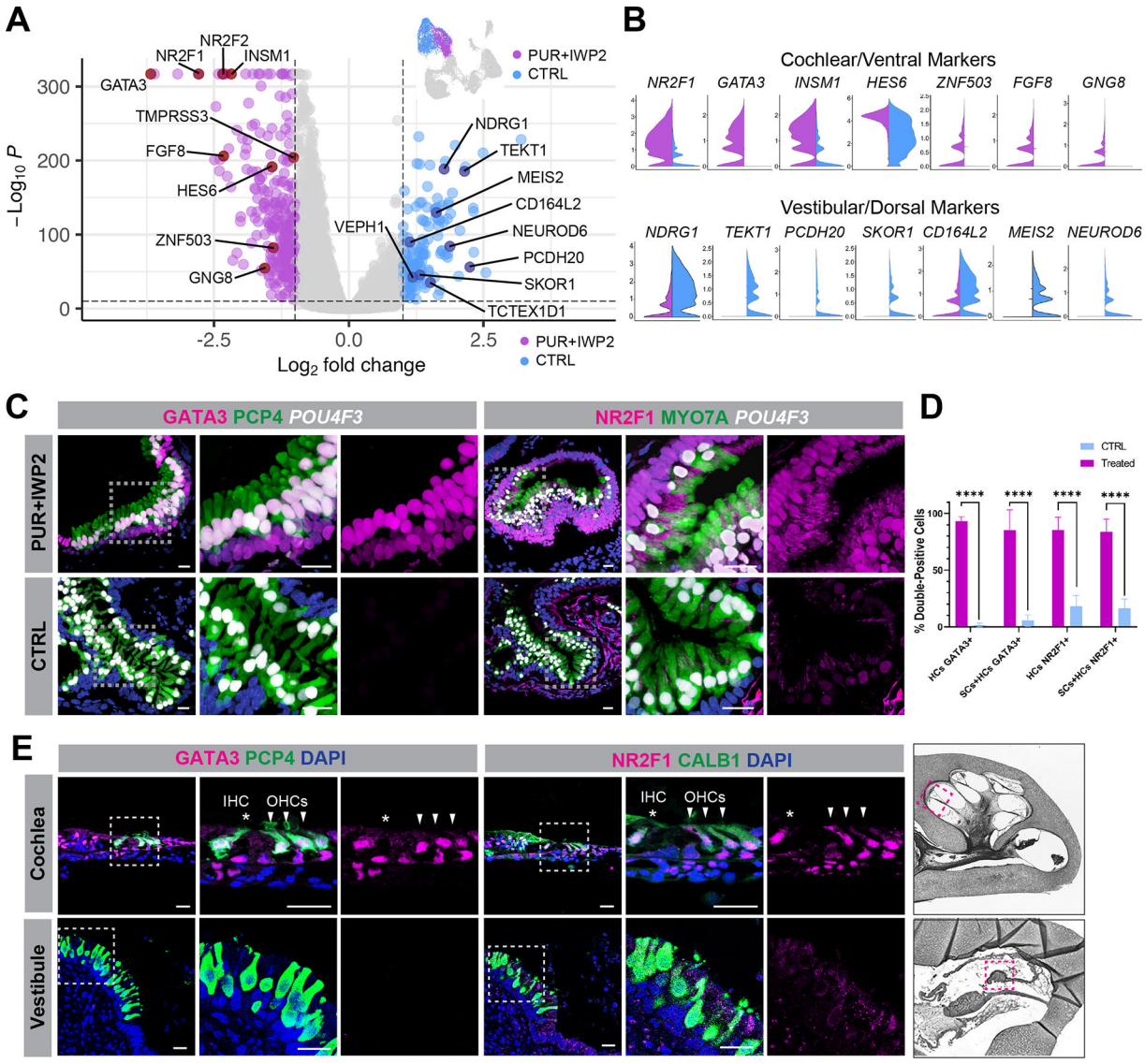

Figure 5. *POU4F3*^{nT}+ cells in ventralized inner ear organoids express cochlear hair cell markers.

(A-B) Volcano plot (A) together with violin plots (B) confirm differentially expressed cochlear and vestibular hair cell marker genes between PUR+IWP2 and CTRL hair cells. Additionally, previously unrecognized genes, such as *NR2F1*, *TMPRSS3*, *CD164L2*, *ZBBX* and *SKOR1*, are differentially expressed between PUR+IWP2 and CTRL hair cells.

(C) Representative immunohistochemistry validates differential expression of NR2F1 and GATA3 between PUR+IWP2 and CTRL organoids.

(D) Comparison of the percentage of NR2F1- or GATA3-positive hair cells (HCs: *POU4F3*^{nT}-labeled) and supporting cells (SCs: SOX2-labeled) in PUR+IWP2 vs. CTRL immunofluorescent images of inner ear organoids; $n = 9$ biological samples from separate experiments; Welch's two-sided t-test ****P<0.000001; values are mean ± SEM.

(E) NR2F1 and GATA3 are expressed in cochlear hair cells, but absent in vestibular hair cells of the crista ampulla in the GW18 human inner ear.

Scale bars, 20 μm (C, E).

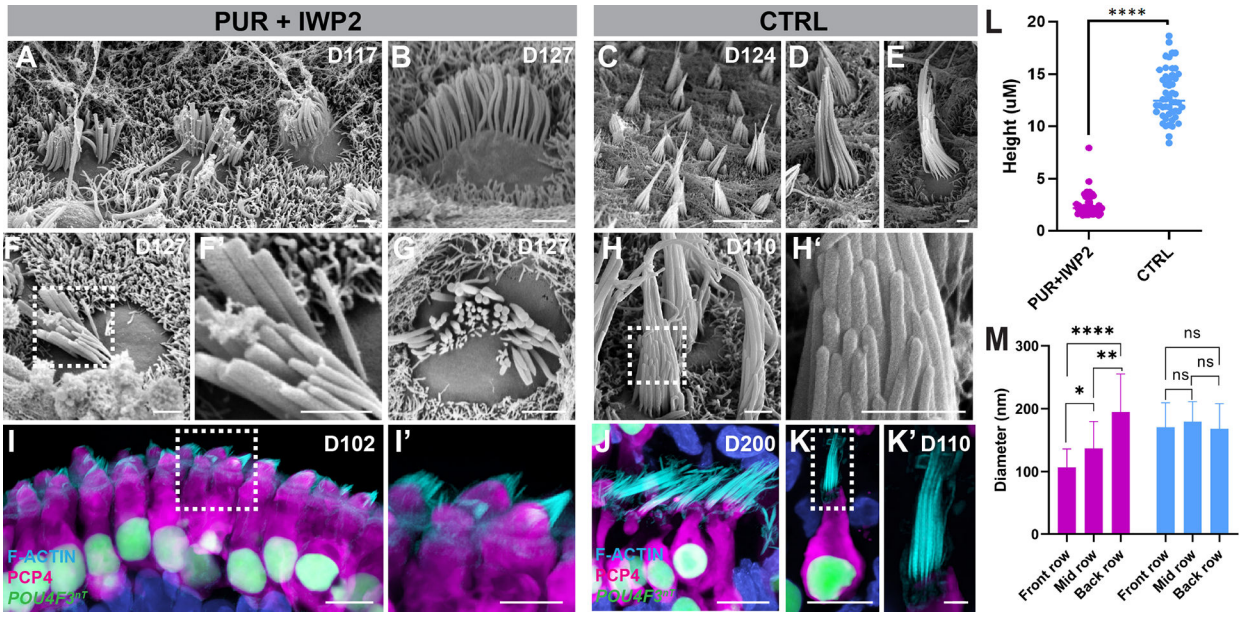

Figure 6. Hair cells derived from ventralized inner ear organoids exhibit structural properties of cochlear hair cells.

(A-H') Scanning electron micrographs of PUR+IWP2 hair bundles (A-B, F-G) reveal relatively short stereocilia organized into concave rows of increasing height and diameter characteristic of a cochlear hair cell phenotype. In contrast, scanning electron micrographs of CTRL hair bundles (C-E, H-H') reveal elongated stereocilia organized into convex rows that are of equivalent diameter characteristic of native vestibular hair cells. i-K', Confocal microscopic images of PUR+IWP2-treated hair cells (I-I') reveal short F-actin^{+} hair bundles and rectangular soma with basally-positioned nuclei, whereas those of CTRL hair cells. (J-K') reveal elongated F-actin^{+} hair bundles and an often-bulbous or flask-shaped soma. CTRL hair cells retain vestibular morphology even at D200 (J).

(L-M) Quantitative analysis of the stereocilia height and the diameter of individual stereocilia in PUR+IWP2 vs. CTRL hair cells; $n = 50$ biological samples from separate experiments: L, Welch's two-sided t-test; M, One-way ANOVA with Tukey' ****P<0.00001; values are mean ± SEM.

Scale bars, 10 μm (C, I, J, K), 1 μm (A, B, D-H, K').

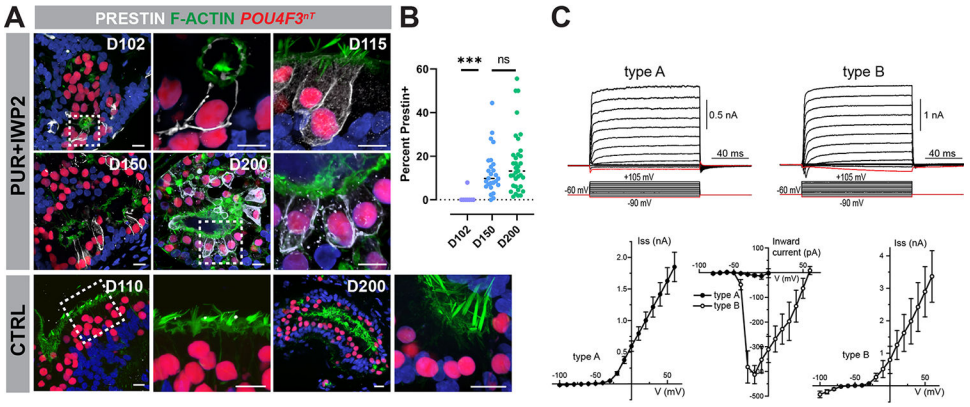

Figure 7. A subpopulation of hair cells derived from ventralized organoids express PRESTIN and exhibit voltage-gated currents characteristic of cochlear outer hair cells.

(A-B) PRESTIN+ hair cells increase over time in PUR+IWP2 inner ear organoids. Representative immunohistochemistry for PRESTIN in PUR+IWP2 samples at D102, −150, and −200, along with the comparison of the percentage of hair cells expressing PRESTIN among the different age groups, reveals an increasing number of hair cells expressing membranous PRESTIN over time in culture. In contrast, PRESTIN is undetectable in CTRL hair cells at D110 or −200.

(C) Voltage-gated currents in hESC-derived hair cells. Typical whole cell current responses (top traces) to the voltage step protocol (bottom traces) in type A and type B cells. Average steady-state current amplitude at the end of voltage step in type A and type B cells. The peak amplitude of the negative inward current. All data are shown as Mean ± Standard Error. Age of the cells: d138-d164.

Scale bars,10 μm (A).

Key resources table

REAGENT or RESOURCE	SOURCE	IDENTIFIER
Antibodies		
CALB1	SWANT	Cat#300
CLDN11	Invitrogen	Cat#36-4500
DLX3	Santa Cruz	Cat#sc-514094
DLX5	Novus Biologicals	Cat#NBP1-85793
FBXO2	Santa Cruz	Cat#sc-398111
GATA3	R&D Systems	Cat#AF2605
GFP	Thermo Fisher	Cat#A-11120
INSM1	Santa Cruz	Cat#sc-271408
LMOD3	Proteintech	Cat#14948-1-AP
LMX1A	Sigma-Aldrich	Cat#AB10533
MYO7A	Proteus	Cat#256790
MYO7A	Santa Cruz	Cat#sc-74516
NDGR1	Abcam	Cat#ab-124689
NR2F1	Invitrogen	Cat#ab-124689
NR2F1	R&D Systems	Cat#PP-H8132-00
OCT4 (conjugated to AF488)	eBioscience	Cat#53584182
OTX2	R&D Systems	Cat#AF1979
PAX2	Abnova	Cat#H00005076-M01
PAX8	Abcam	Cat#AB97477
PCP4	Santa Cruz	Cat#sc-74816
PCP4	Invitrogen	Cat#PA5-52209
phalloidin (conjugated to AF488)	Thermo Fisher	Cat#A12379
POU4F3	Santa Cruz	Cat#sc-81980
Prestin	Generous gift of Drs. Jing Zheng and Kazuaki Homma et al.[28]	NW-802
Sox10	eBioscience	Cat#14-5923-82
Sox2	BD Pharmingen	Cat#561469
SSEA4 (conjugated to AF594)	BioLegend	Cat#330414
SULF1	Invitrogen	Cat#PA5-113112
TUBA4A	Sigma-Aldrich	Cat#T6793
TUJ1 (TUBB3)	Biolegend	Cat#801201
Bacterial and virus strains		
DH5a	New England Biolabs	Cat#C2987H
Biological samples		
GW 13 Human fetal cochlea	This paper	N/A
GW 18 Human fetal cochlea	This paper	N/A
GW 18 Human fetal vestibule	This paper	N/A

REAGENT or RESOURCE	SOURCE	IDENTIFIER
Chemicals, peptides, and recombinant proteins		
Accutase	Thermo Fisher Scientific	Cat# A1110501
Advanced DMEM/F12	Thermo Fisher Scientific	Cat#12634028
Alt-R™ S.p. Cas9 Nuclease V3	Integrated DNA technologies (IDT)	Cat#1081058
B27 (minus vitamin A)	Thermo Fisher Scientific	Cat#12587010
β-Mercaptoethanol	Thermo Fisher Scientific	Cat#21985023
BMP4	Reprocell	Cat#03-0007
CHIR99021	Reprocell	Cat#04-0004-10
DMEM/F12 +HEPES	Thermo Fisher Scientific	Cat#11320033
DPBS	Thermo Fisher Scientific	Cat#14040133
Essential 6 (E6) medium	Thermo Fisher Scientific	Cat#A1516401
Essential 8 (E8) Flex medium	Thermo Fisher Scientific	Cat#A2858501
0.5 M EDTA, pH 8.0	Thermo Fisher Scientific	Cat#15575020
FGF2	Stem Cell Technologies	Cat#780003
GFR Matrigel	Corning	Cat#354230
GlutaMAX	Thermo Fisher Scientific	Cat#35050061
Glutaldehyde	Electron Microscopy Sciences (EMS)	Cat#16537-15
IWP-2	Tocris	Cat#3533
LDN193189	Stemgent	Cat#04-0074-02
L-15 cell culture medium	Thermo Fisher Scientific	Cat#21083027
Neurobasal medium	Thermo Fisher Scientific	Cat#21103049
Normocin	Invivogen	Cat# ant-nr-1
N2	Thermo Fisher Scientific	Cat#17502048
Osmium tetroxide	Electron Microscopy Sciences (EMS)	Cat#19150
Propidium Iodide	Invitrogen	Cat#P1304MP
Purmorphamine	Stemgent	Cat#04-0009)
RevitaCell	Thermo Fisher Scientific	Cat#A2644501
SB431542	Stemgent	Cat#04-0010-05
Scr7	Xcessbio	Cat#M60082-2S
TRIzol	Thermo Fisher Scientific	Cat#15596026
TrypLE	Thermo Fisher Scientific	Cat#A1217701
Vitronectin-N	Thermo Fisher Scientific	Cat#A14700
Y-27632	Stemgent	Cat#04-0012-02
Critical commercial assays		
Chromium Next GEM Single Cell Kit v3	10x Genomics	Cat#1000075
Deposited data		
Raw and analyzed data	This paper	GEO: GSE200629
Experimental models: Cell lines		
WA25	WiCell	(NIHhESC-12-0196; RRID:CVCL_E080)

REAGENT or RESOURCE	SOURCE	IDENTIFIER
mND2-0	WiCell	mND2-0 (MIRJT7i-mND2-0,RRID:CVCL_U173)
Oligonucleotides		
PAX2 RT assay Fwd: CCTGGCAGGAATGGTGCCT	This paper	N/A
PAX2 RT assay Rev: GTCAGACGGGGACGATGTGG	This paper	N/A
Primers for PAX2 donor vector: see supplementary table 2	This paper	N/A
Primers for POU4F3 donor vector: see supplementary table 2	This paper	N/A
PAX2 gRNA: ATGACCGCCACTAGTTACCG	This paper	N/A
POU4F3-targeting sgRNA for CRISPR/Cas9 genome editing: ATTCGGCTGTCCACTGATTG	This paper	N/A
Recombinant DNA		
SpCas9-HF1 vector	Kleinstiver et al.[14]	Addgene#72247
U6 expression vector	Slaymaker et al.[55]	Addgene #71814
Cre expression vector	Matsuda et al.[57]	Addgene #13775
FLPo expression vector	Raymond et al.[58]	Addgene #13793
2A-eGFP-PGK-Puro vector	Hockemeyer et al.[54]	Addgene #31938
Software and algorithms		
ImageJ	Schneider et al.[59]	https://imagej.nih.gov/ij/
Flow Jo	FlowJo LLC	https://www.flowjo.com/
Prism 9	GraphPad Software	https://graphpad.com
Imaris 8	Bitplane	https://Imaris.oxinst.com/
R	Team R C. R: A language and environment for statistical computing[J]. 2013.	https://cran.r-project.org/bin/macosx/ (macOS)https://cran.r-project.org/bin/windows/base/ (Windows)https://cran.r-project.org/bin/linux/ (Linux)
R studio	Team R S. Rstudio: integrated development for R[J]. Rstudio, Inc., Boston, MA URL http://www.Rstudio.com, 2015, 42: 14.	https://www.rstudio.com/products/rstudio/download/
R package Seurat		https://github.com/satijalab/seurat
DESeq2	Love et al.[62]	https://bioconductor.org/packages/release/bioc/html/DESeq2.html
zingeR	Love et al.[62]	https://github.com/statOmics/zingeR/blob/master/R/methods.R
iDEA	Ma et al.[21]	https://xzhoulab.github.io/iDEA/
Custom code	This paper	https://github.com/HashinoLab/Moore_et¬_al_Cochlear_Organoids
Nikon Elements microscope imaging software	Nikon Corporation	https://www.nikoninstruments.com/Products/Software/NIS-Elements-Advanced-Research/NIS-Elements-Viewer